Cell

Tau PTM Profiles Identify Patient Heterogeneity and Stages of Alzheimer's Disease

Graphical Abstract

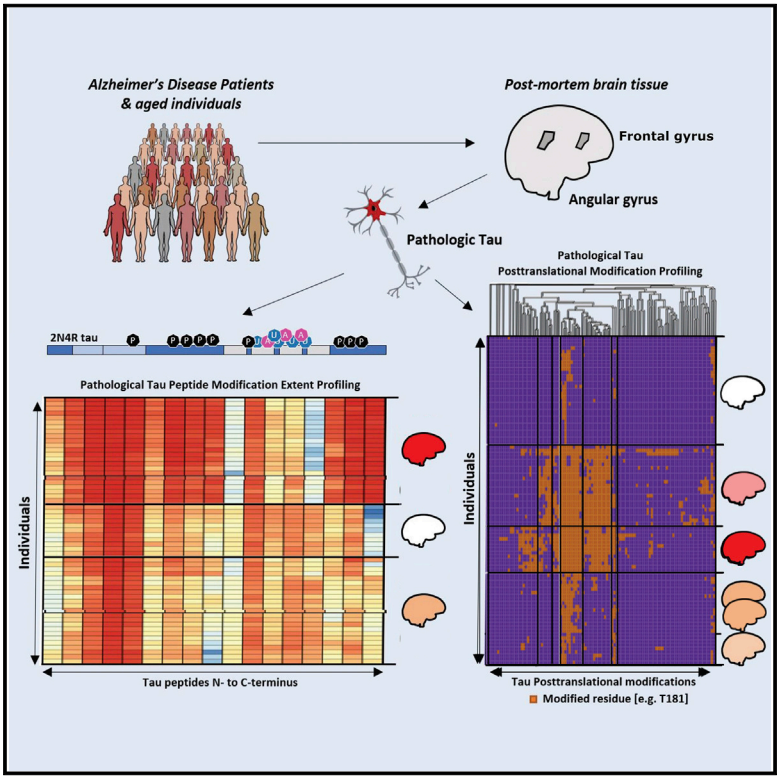

Highlights

- 95 post-translational modifications (PTMs) were identified on Tau in human subjects
- Frequency and PTM stoichiometry of pathological Tau identify patient heterogeneity
- Modifications occur in a processive fashion and are reflective of disease progression
- The study identifies critical therapeutic targets at each stage of disease

Authors

Hendrik Wesseling, Waltraud Mair, Mukesh Kumar, ..., Bradley T. Hyman, Hanno Steen, Judith A. Steen

Correspondence

judith.steen@childrens.harvard.edu

In Brief

A high-resolution quantitative proteomics map of post-translational modifications on multiple isoforms of Tau shows heterogeneity across Alzheimer's disease patients, reflective of disease progression, and identifies critical targets at each stage of disease.

Wesseling et al., 2020, Cell *183*, 1–15
December 10, 2020
https://doi.org/10.1016/j.cell.2020.10.029

CellPress

Please cite this article in press as: Wesseling et al., Tau PTM Profiles Identify Patient Heterogeneity and Stages of Alzheimer's Disease, Cell (2020), https://doi.org/10.1016/j.cell.2020.10.029

Cell

CellPress

Resource

Tau PTM Profiles Identify Patient Heterogeneity and Stages of Alzheimer's Disease

Hendrik Wesseling,[1,10] Waltraud Mair,[1,10] Mukesh Kumar,[1] Christoph N. Schlaffner,[1] Shaojun Tang,[1,2] Pieter Beerepoot,[1] Benoit Fatou,[2] Amanda J. Guise,[1] Long Cheng,[1] Shuko Takeda,[3,4] Jan Muntel,[2] Melissa S. Rotunno,[2] Simon Dujardin,[3] Peter Davies,[9] Kenneth S. Kosik,[5] Bruce L. Miller,[6] Sabina Berretta,[8] John C. Hedreen,[8] Lea T. Grinberg,[6,7] William W. Seeley,[6,7] Bradley T. Hyman,[3] Hanno Steen,[2] and Judith A. Steen[1,11,*]

[1]F.M. Kirby Neurobiology Center, Department of Neurobiology, Boston Children's Hospital, Harvard Medical School, Boston, MA 02115, USA
[2]Department of Pathology, Boston Children's Hospital, Harvard Medical School, Boston, MA 02115, USA
[3]Department of Neurology, Massachusetts General Hospital, Harvard Medical School, Charlestown, MA 02129, USA
[4]Department of Clinical Gene Therapy, Graduate School of Medicine, Osaka University, Yamadaoka, Suita, Osaka 565-0871, Japan
[5]Neuroscience Research Institute and Department of Molecular, Cellular, and Developmental Biology, UCSB, Santa Barbara, CA 93106, USA
[6]Department of Neurology, Memory and Aging Center, University of California, San Francisco, San Francisco, CA 94143, USA
[7]Department of Pathology, University of California, San Francisco, San Francisco, CA 94143-0511, USA
[8]Harvard Brain Tissue Resource Center (HBTRC), McLean Hospital, Belmont, MA 02478, USA
[9]Feinstein Institutes for Medical Research, Manhasset, NY 11030, USA
[10]These authors contributed equally
[11]Lead Contact
*Correspondence: judith.steen@childrens.harvard.edu
https://doi.org/10.1016/j.cell.2020.10.029

SUMMARY

To elucidate the role of Tau isoforms and post-translational modification (PTM) stoichiometry in Alzheimer's disease (AD), we generated a high-resolution quantitative proteomics map of 95 PTMs on multiple isoforms of Tau isolated from postmortem human tissue from 49 AD and 42 control subjects. Although Tau PTM maps reveal heterogeneity across subjects, a subset of PTMs display high occupancy and frequency for AD, suggesting importance in disease. Unsupervised analyses indicate that PTMs occur in an ordered manner, leading to Tau aggregation. The processive addition and minimal set of PTMs associated with seeding activity was further defined by analysis of size-fractionated Tau. To summarize, features in the Tau protein critical for disease intervention at different stages of disease are identified, including enrichment of 0N and 4R isoforms, underrepresentation of the C terminus, an increase in negative charge in the proline-rich region (PRR), and a decrease in positive charge in the microtubule binding domain (MBD).

INTRODUCTION

Alzheimer's disease (AD) is associated with aging and results in devastating disability and diminished quality of life; its occurrence will reach epidemic proportions by 2050 if not abated. The pathological hallmarks of AD are the two proteins β-amyloid (Aβ) and Tau. Aβ forms extracellular plaques (Glenner and Wong, 1984; Masters et al., 1985), whereas Tau forms intracellular neurofibrillary tangles (NFTs) (Grundke-Iqbal et al., 1986; Kosik et al., 1986; Wood et al., 1986). Although many studies have shown the importance of Aβ, therapeutic efforts targeting Aβ have not been successful, shifting the focus to Tau. The discovery of dominantly inherited Tau mutations leading to frontotemporal dementia (FTD) (Poorkaj et al., 1998; Spillantini et al., 1998) and correlation of Tau pathology with cognitive decline in AD (Arriagada et al., 1992; Bierer et al., 1995; Giannakopoulos et al., 2003; Gómez-Isla et al., 1997) have led to several mechanistic studies whose outcomes have underscored the importance of Tau in AD and other dementias (Mudher et al., 2017). Since the discovery of phosphorylation and the first description of isoforms of Tau (Cleveland et al., 1977), the roles of Tau proteoforms (different chemical versions of a polypeptide) have been explored functionally (Adams et al., 2010), and many of these studies have highlighted the importance of post-translational modifications (PTMs) of Tau in AD and FTD (Bramblett et al., 1993; Min et al., 2010).

During disease progression in AD, pathological neurofibrillary Tau aggregates show a pattern of accumulation that starts in the entorhinal cortex and spreads through connected pathways to cortical areas (Jucker and Walker, 2013). This encompasses a cycle that involves production of a Tau seed followed by uptake of seed-competent Tau into connected cells (Clavaguera et al., 2013). This seeding of soluble Tau in recipient neurons and propagation of Tau aggregates by release of Tau seeds into the extracellular space (de Calignon et al., 2012) has been called prion-like (Walker et al., 2013). It has been suggested that brain lysates seed Tau aggregation when high-molecular-weight (HMW) oligomeric hyperphosphorylated (AT8 and AT100) Tau species are

Please cite this article in press as: Wesseling et al., Tau PTM Profiles Identify Patient Heterogeneity and Stages of Alzheimer's Disease, Cell (2020), https://doi.org/10.1016/j.cell.2020.10.029

present (Takeda et al., 2015; Jackson et al., 2016). Besides phosphorylation, the neurofibrillary aggregates are also subject to a wide range of other PTMs (Hanger et al., 2007). Thus, it has been hypothesized that the types of PTMs, their site-specific localization, and their extent of modification induce or mediate Tau aggregation and propagation (Cohen et al., 2011; Alonso et al., 2001). Profiling the specific molecular characteristics of pathological Tau in human AD is critical for early diagnosis and development of mechanism-directed therapies.

A protein can be modified by PTMs, giving rise to different proteoforms (Smith et al., 2013). Combinations of such PTMs are responsible for regulating and fine-tuning protein conformation and activity (Aebersold et al., 2018; Soria et al., 2014) and can dramatically change the function and toxicity of proteins. To effectively understand the functional significance of protein modification, all possible PTMs should be mapped from the N to the C terminus. Although several PTMs are present at basal levels in cells, not all of these are functionally significant in the context of specific pathological conditions (Singh et al., 2014). Thus, to understand the function of a particular PTM, it is equally important to obtain information about PTM stoichiometry.

Knowledge of human Tau in disease and health is important for development of diagnostics such as Positron Emission Tomography (PET) reagents and therapeutic agents. For example, to develop a Tau PET radiotracer for detection of disease before cognitive decline, the chemical composition and abundance of pathological species at early disease stages is essential (Brosch et al., 2017). In addition, knowledge of the pattern of Tau PTMs on the pathologic species would allow improvement of PET reagent affinities for Tau. Defining the chemistry of the pathologic Tau proteoforms during progression of disease will allow us to target specific epitopes using therapeutic antibodies or small molecules at every stage of disease. Furthermore, the minimum set of PTMs important for oligomer formation and Tau aggregation is not known. Finally, it is not known which PTMs occur on Tau seeds that can potentiate further aggregation. The mechanistic role of PTMs in initiating Tau seeding and propagation still remains to be elucidated (Guo et al., 2017; Wang and Mandelkow, 2016).

Immunohistochemistry has been the workhorse for identification and quantification of Tau proteoforms. Although such antibody-based approaches are simple to implement and provide semiquantitative information, they cannot accurately measure quantitative changes or determine PTM stoichiometry. Finally, all antibody-based approaches require *a priori* knowledge of sites and cannot be used for discovery purposes. To overcome these issues, we previously developed a targeted, high-throughput quantitative mass spectrometry (MS) method called FLEXITau (full-length expressed stable isotope-labeled Tau) (Mair et al., 2016), which provides absolute quantification and unbiased stoichiometric information of Tau PTMs from the N to the C terminus. Tens of possible PTM sites have been described for Tau in studies involving *in vitro* (Hanger et al., 2007; Martin et al., 2013a, 2013b) and *in vivo* AD mouse models (Morris et al., 2015; Tramutola et al., 2018) and in postmortem human studies (Hanger et al., 2007; Min et al., 2015). To our knowledge, a qualitative and quantitative approach using a large cohort of human AD subjects has not been performed. Obtaining data from a large cohort of patients could allow us to understand which combinations of specific PTMs can contribute to seeding and aggregation and better understand the mechanisms of oligomer and fibril formation. Although mapping these PTMs is important, specifying the PTMs that contribute to fibril formation as well as propagation of seeding is key to prevent formation of Tau fibrils. In this study, we had multiple aims, including determining the absolute quantities (molar concentrations) of pathologic Tau in AD, providing a comprehensive map of PTMs in human AD, determining the distribution of isoforms of Tau in the pathologic and non-pathologic forms of Tau, and understanding the extent (stoichiometry) of modification and the heterogeneity of modification profiles across AD patients and control (CTR) subjects.

To understand the importance of PTMs in disease, a comprehensive analysis of PTMs in a cohort requires numerous levels of information, including (1) the type of PTM, (2) PTM localization, (3) PTM frequency in the subject cohort, and (4) PTM stoichiometry. Thus, quantitative and qualitative protein profiling of human tissues (n = 91) was performed. FLEXITau and unbiased MS-based proteomics were used to characterize and map the PTM landscape of pathological Tau for AD. We then used supervised and unsupervised data analyses to determine the most relevant molecular features of Tau pathology that are important in Tau aggregation. Further, we studied size-resolved fractions of Tau to identify the minimal set of PTMs associated with seeding potential and the role of PTMs in the ontogeny of fibril formation. These qualitative and quantitative data provide key insights into the role of PTMs in the progression of disease and identification of key targets for development of therapeutic antibodies, imaging reagents, and diagnostics for AD.

RESULTS

Multiple types of qualitative and quantitative MS analyses were employed to characterize the molecular features of Tau from the BA39 angular gyrus region in postmortem brain tissue from two cohorts with overlapping subjects comprised of 49 AD patients and 42 age-, postmortem interval (PMI)-, and sex-matched control subjects (Tables S1 and S2). The subjects were selected based on the criterion of diagnosis prior to death as being clinical AD or were asymptomatic (controls). The next criterion was definitive postmortem neuropathological final diagnosis by the respective brain banks as AD or unaffected. Selected subjects had the least possible concurrent pathologies and were assessed for Braak NFT stages (Braak and Braak, 1991), as determined by the location of NFTs with total Tau immunostaining and Bielschowsky's silver stain. Inclusion in the study required a high-confidence postmortem neuropathological diagnosis of AD, based on relevant criteria (Montine et al., 2016; Mirra et al., 1991), for the clinical AD group or no more than low AD neuropathological change (Montine et al., 2016) or a Braak stage of less than IV for the clinical control group. Principal-component analysis (PCA) analysis did not show any effect of age, PMI, or sex on the Tau PTM profiles for both cohorts (Figure S1). The angular gyrus was selected as a brain region of intermediate pathology in the end stage of disease without a large amount of neuronal loss. To determine whether similar Tau PTMs and

Please cite this article in press as: Wesseling et al., Tau PTM Profiles Identify Patient Heterogeneity and Stages of Alzheimer's Disease, Cell (2020), https://doi.org/10.1016/j.cell.2020.10.029

quantitative profiles were observed in other affected brain regions, we analyzed the molecular features of Tau from the frontal gyrus (BA46) region in 9 control and 10 AD patients (Table S2) using complementary analysis. A schematic overview of cohort selection, sample preparation, and MS analysis is shown in Figure 1A. The data and subsequent analyses showed that the highest-frequency PTMs, isoform distributions, and quantitative profiles of the BA46 region are shared between the two brain regions (see below and Figure S2).

Tau Concentrations and Isoform Distributions in AD and Control Subjects

FLEXITau was employed to determine the molar concentration (absolute quantification) of Tau from sarkosyl-soluble and insoluble fractions of cortical gray matter from the parietal lobe association cortex (BA39). The total amount of soluble Tau is lower in AD patients (~3,000 fmol/mg fresh weight of tissue) compared with control subjects (~5,000 fmol/mg fresh weight of tissue) (Figure 1B). The median concentrations of pathological insoluble Tau in BA39 were 100-fold higher in AD (~1,000 fmol/mg fresh weight of tissue) compared with controls (~10 fmol/mg fresh weight of tissue) (Figure 1B). It is important to note that insoluble Tau also accumulated in the age-matched control subjects, albeit at lower concentrations. FLEXITau quantified a total of 24 Tau peptides; of these, some were isoform specific, achieving a total sequence coverage of 61% for the 2N4R Tau isoform (Figure 1D). Relative quantities of the 0N, 1N, 2N, 3R, and 4R Tau isoform-specific peptides were measured in the soluble and insoluble fractions (Figure 1C). Interestingly, in soluble Tau, the most abundant species are the 1N and 4R isoforms, whereas in the insoluble fraction containing pathologic Tau, 0N and 1N Tau were enriched significantly compared with the 2N isoform, and the 4R isoform is enriched significantly compared with the 3R isoform. Absolute quantification of Tau isoforms shows that the distribution of different isoforms in the soluble fractions is not mirrored in the pathological insoluble fraction that contains the fibrils. Instead, the 1N isoform is depleted significantly, and the 0N isoform is enriched in the insoluble fraction. These data suggest that the 0N and 4R isoforms are more prone to aggregation in AD, and these findings were also recapitulated in sarkosyl-insoluble Tau extracts from BA46 (Figure S2A).

Qualitative and Quantitative Maps of Tau PTMs and Their Frequency in AD Patient

Qualitative and quantitative analysis of all Tau isoforms in two different cohorts and two different brain regions identified (1) the types of PTMs, (2) PTM localization, (3) PTM subject frequency, and (4) PTM stoichiometry based on the FLEXITau profile. We identified 95 distinct PTMs on 88 amino acid residues across all samples and fractions, with a cumulative sequence coverage of 96% from detected modified and unmodified 2N4R Tau peptides (Figure 1E). Details of all modified peptides, including statistical peptide confidence score (Table S3), patient frequency (Table S4) and whether the modification is unique to humans (Table S5), are provided. Although 86 phosphorylation events have been described on Tau in general (Arendt et al., 2016) (i.e., *in vivo*, *in vitro*, and across different organisms and model systems), and over 31 phosphorylation sites have been identified to be associated with physiological functions (Hasegawa et al., 1992; Lovestone and Reynolds, 1997; Morishima-Kawashima et al., 1995), only 45 Tau phosphorylation events have so far been described on pathological human Tau (Arendt et al., 2016); that is, Tau analyzed from primary human specimens. Our analysis extended this to 55 phosphorylation sites on pathological insoluble Tau in BA39 and 43 phosphosites in B46 (Figure S2C). A total of 28 ubiquitination sites have been identified previously on Tau extracted from postmortem AD brain total lysates using ubiquitination enrichment (Abreha et al., 2018). In this study, we show that 17 ubiquitin sites are specific to pathological Tau (14 in BA46; Figure S2C). Sixteen of 17 identified ubiquitination sites are in the microtubule binding domain (MBD), which forms the core of the filament (Crowther et al., 1989; Falcon et al., 2018; Fitzpatrick et al., 2017). Nineteen distinct acetylation sites were mapped in BA39 and 18 in BA46. Interestingly, some of these acetylation sites are also ubiquitinated in pathological Tau. Four methylation sites were also detected.

The patient frequencies of these 95 PTMs are shown in Figure 1F (for BA46, see Figure S2C), where we compare insoluble Tau from AD and control subjects. Frequency is key to understanding the pathology of the different PTMs and the heterogeneity of the patient population. Some of the 88 sites of modification mapped are modified by a single type of PTM; however, others can carry multiple types of modifications, such as K311, which can be ubiquitinated or acetylated. There are multiple sites that are observed in one or two patients in both cohorts and therefore are less likely to be relevant to disease, such as phosphorylation at S113. Heatmaps of the median peptide modification extent from the FLEXITau MS data (cohorts 1 and 2) are overlaid with the frequency data to evaluate the stoichiometry of the PTMs. PTMs known to be significant and correlated with disease, such as the AT8 epitope containing the phosphorylation sites S199, S202, and T205, are found with high frequency and high stoichiometry in the patient population. Given this, the most relevant PTMs are the ones that show high frequency and extent of modification in AD subjects.

A high frequency of acetylation occurs in the R4 region, including the sites K353, K369, K370, and K375, whereas ubiquitination occurs in R1–R3. This is also reflected in the frontal gyrus (BA46) (Figure S2C). Interestingly, in R3, the hexapeptide VQIVYK at site K311 shows acetylation and ubiquitination, with increased propensity for ubiquitination. In Figure 1F, the FLEXITau data shown below the frequency graph displays the extent of modification of the PTMs for 49 AD and 42 control patients and aligns with the PTM frequencies.

Phosphorylation sites cluster with highest frequency in the proline-rich region (PRR). In particular, the peptides spanning (195-209) and (212-224) that encompass the sites (S198, S199, S202, T205) and (S212, S214, S217) respectively, are observed to be > 90% modified in AD in the FLEXITau data. In addition, the region spanning amino acid residues [396-406] features high frequency phosphorylation at S396, S400, T403, and at S404 and show > 90% modification extent (Figure 1F). This observation is also true for BA46 (Figure S2C). Interestingly, for both brain regions (Figures 1F; Figure S2C), there are some

Please cite this article in press as: Wesseling et al., Tau PTM Profiles Identify Patient Heterogeneity and Stages of Alzheimer's Disease, Cell (2020), https://doi.org/10.1016/j.cell.2020.10.029

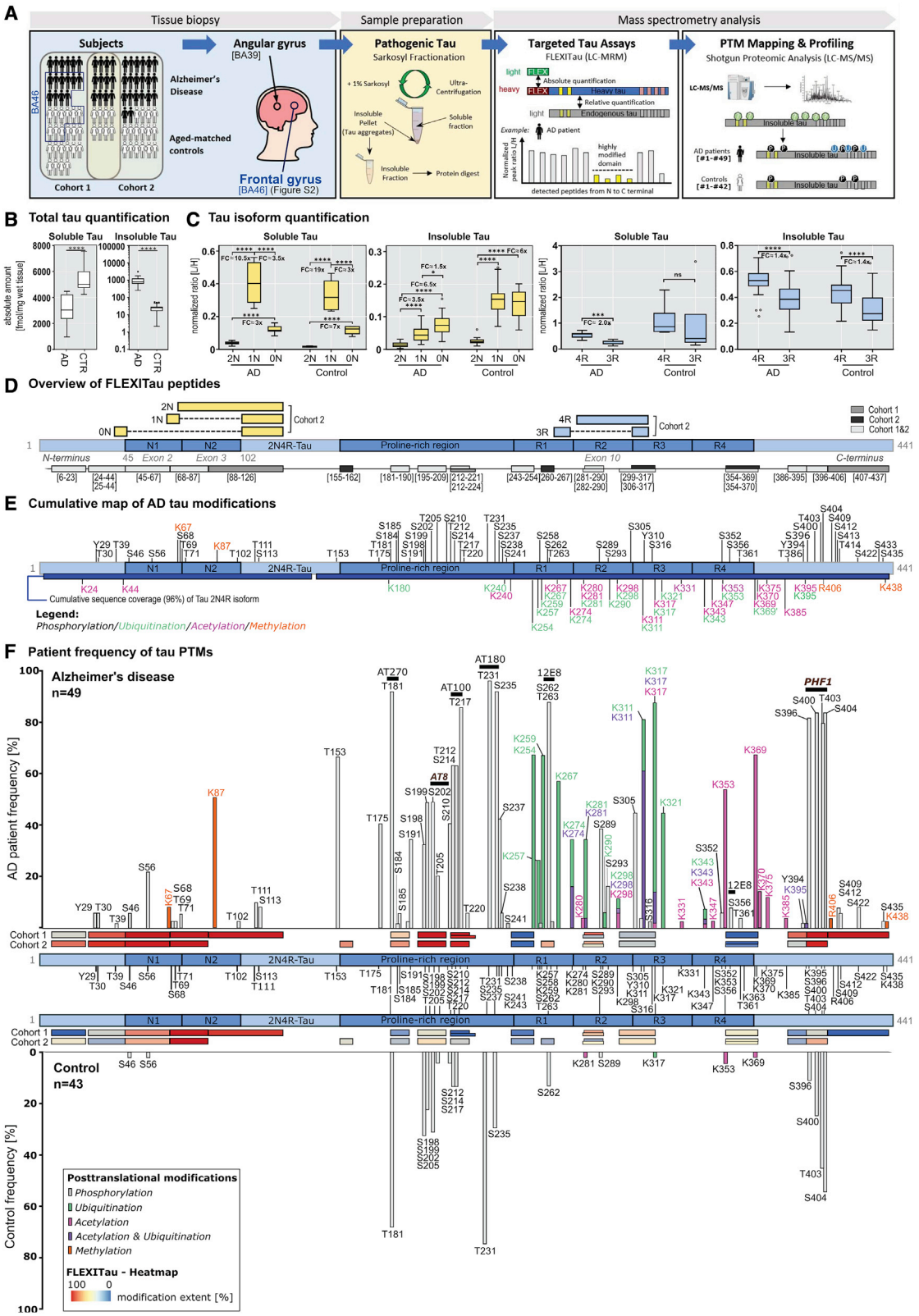

(legend on next page)

Please cite this article in press as: Wesseling et al., Tau PTM Profiles Identify Patient Heterogeneity and Stages of Alzheimer's Disease, Cell (2020), https://doi.org/10.1016/j.cell.2020.10.029

high-frequency PTMs in insoluble Tau from controls such as T181 and T231. In some control subjects, these phosphopeptides are further phosphorylated and show some of the same PTMs associated with pathological Tau (Goedert et al., 1995). These phosphorylation sites at S198, S199, S202, T205 in the peptide (195-209) are observed in 20%–40% of the controls, suggesting that early disease is observed in a few controls.

Individual Tau PTM Profiles Show Heterogeneity and Reflect Disease Progression

Figure 2A depicts the unsupervised hierarchical clustering analyses of Tau PTMs identified in AD and control subjects across the two cohorts. The left panel shows the PTMs as clustered by PTM features, whereas the right panel shows the PTM features arranged from the N terminus to the C terminus of Tau. Information about clinical and pathological diagnosis as well as Braak staging (Braak and Braak, 1991) is provided on the left of the figure for subjects where data were available (23 AD and 27 controls). In addition, the levels of Aβ and Tau measured in each sample are shown (pink and blue heatmap). ANOVA analysis showed higher Tau and Aβ levels in clusters with a higher Braak stage and increased level of Tau PTMs (Figure 2B). A large percentage of AD patients cluster into two major groups (Figure 2A, **b** and **c**), whereas the controls fall into two clusters (Figure 2A, **a** and **d**).

The control cluster **a** has the lowest number of PTMs and we observe the peptide (225-242) with single phosphorylation at (S231 or S235) and some subjects with phosphorylation at T181. This cluster **a** is largely comprised of patients staged Braak 0–III. Cluster **d** differs from by occurrence of phosphorylation at epitopes identified by the AT8 antibody (**d**-**V**: S199 and S202), the PHF1 antibody (**d**-**III**: S396, S400, T403, and S404), the AT120 antibody (**d**-**III**: T212 and T217), and the single S262 phosphorylation. Tau from cluster **a** control subjects displays phosphorylation sites that are associated with normal physiological function, whereas controls in cluster **d** show additional sites associated with pathology. The majority of subjects in **d** are listed as control subjects, and these PTMs are likely to be the earliest signs of pathology. Cluster **d** contains 10 symptomatic patients with late stage AD pathology Braak IV-VI and 16 asymptomatic controls at Braak 0–II. The 10 symptomatic patients show some ubiquitination in the MBD domain and this may be the defining feature for symptomatic patients. The 16 asymptomatic patients display increased phosphorylation of the PRR, such as T181, which has been reported to be increased in antemortem plasma of individuals with mild cognitive impairment (MCI) (Janelidze et al., 2020; Thijssen et al., 2020). Increased phosphorylation of the PRR is also observed in symptomatic patients in cluster **d** as well as in AD clusters **b** and **c**; thus, although patients were not diagnosed as symptomatic, they may have shown early cognitive defects at the time of death. The majority of AD patients separates into clusters **b** and **c** and a minority cluster with the control cluster **d**, who show some early pathology. Some clinically asymptomatic subjects in cluster **d** show feature **III** PTMs associated with AD.

The Braak stage of cluster **b** is V, whereas the Braak stage of cluster **c** is VI, and subjects in these clusters have a significantly higher Tau and amyloid burden in BA39 than subjects falling into clusters **a** and **d** (Figure 2B). The hallmarks of clusters **b** and **c** are PTMs in the MBD domain labeled **IV**. These PTMs include phosphorylation occurring at adjacent sites (S262 and S263), acetylation (K311, K353, and K369), and ubiquitination (K259, K267, K311, and K317). These PTMs are not identified in any of the other clusters. Phosphosites previously identified in cluster **d** in the PRR (S231, S235, S212, and S217) and the PHF1 epitope (S396, S400, T403, and S404) are highly populated in clusters **b** and **c**. Clusters **b** and **c** display many of the same PTMs; however, in cluster **c**, we observe a higher frequency of several PTMs, including T175, S237, and K281 (and S113, S191, and T205, which are difficult to observe at lower stoichiometry, particularly because S113 is a phosphosite found on a 0N Tau peptide). The higher occupancy in **I**, **II**, and **IV** PTMs at T175, S237, and K281 is associated with symptomatic late-stage disease (Braak stage VI).

We used partial least-squares discriminant analysis (PLS-DA) to determine which of the robustly quantifiable post-translationally modified peptides are most important for separation of the AD and control groups (Figure 2C). The analysis provides a variable importance in projection (VIP) score that provides a measure of the importance of each modified peptide for

Figure 1. Molecular Characterization of the Isoform Distribution and PTMs of Sarkosyl-Soluble and Insoluble Tau Extracted from Postmortem Angular Gyrus (BA39) Tissues from AD and Healthy Controls (CTR)

(A) Schematic overview of the study and workflow.

(B) Total absolute insoluble Tau abundance, quantified by FLEXITau, is significantly higher in AD than in controls (t test) whereas the soluble Tau counterpart is lower in AD than in controls (t test).

(C) Isoform composition of sarkosyl-insoluble Tau from human angular gyrus tissue shows that pathogenic Tau aggregates are predominately composed of the 0N and 1N isoforms (yellow boxplot) and 4R isoform (blue boxplot) across the tauopathy disease spectrum, whereas 1N and 4R are the predominant forms in the sarkosyl-soluble fraction. Peptides were quantified using heavy-isotope-labeled, isoform-specific peptides, and ANOVA (Kruskal-Wallis) was performed, using Dunn's test for multiple comparisons. Fold changes were calculated based on the mean of the concentrations measured.

(D) An overview of peptide coordinates of Tau, including isoform-specific peptides measured in the targeted quantitative FLEXITau assays. Isoform-specific regions are shown in yellow and blue. Amino acid positions for peptides are projected onto the 2N4R sequence of Tau in parentheses.

(E) Cumulative PTM map of all MS-analyzed Tau species (soluble, insoluble, LMW, HMW, and MC1-isolated Tau) extracted from AD brain tissue (BA39 and BA46).

(F) The patient frequencies of PTMs from the N to the C terminus of Tau show a wide range of frequencies from 2%–90% for AD. Some high-frequency sites are known AD epitopes, such as the 202–205 phosphorylation site (AT8 antibody), pinpointing important PTM-specific sites. Interestingly, some of the-high frequency PTMs, particularly in the MBD, have not been described as being important for pathological Tau. Antibodies commonly used in Tau biology are annotated, and antibodies used for pathology diagnosis are depicted in brown. FLEXITau heatmaps of median peptide modification extent are overlayed with the frequency data to evaluate the stoichiometry of PTMs.

p-value: ****p<0.0001; ***p<0.001; **p<0.01; *p<0.1.

Please cite this article in press as: Wesseling et al., Tau PTM Profiles Identify Patient Heterogeneity and Stages of Alzheimer's Disease, Cell (2020), https://doi.org/10.1016/j.cell.2020.10.029

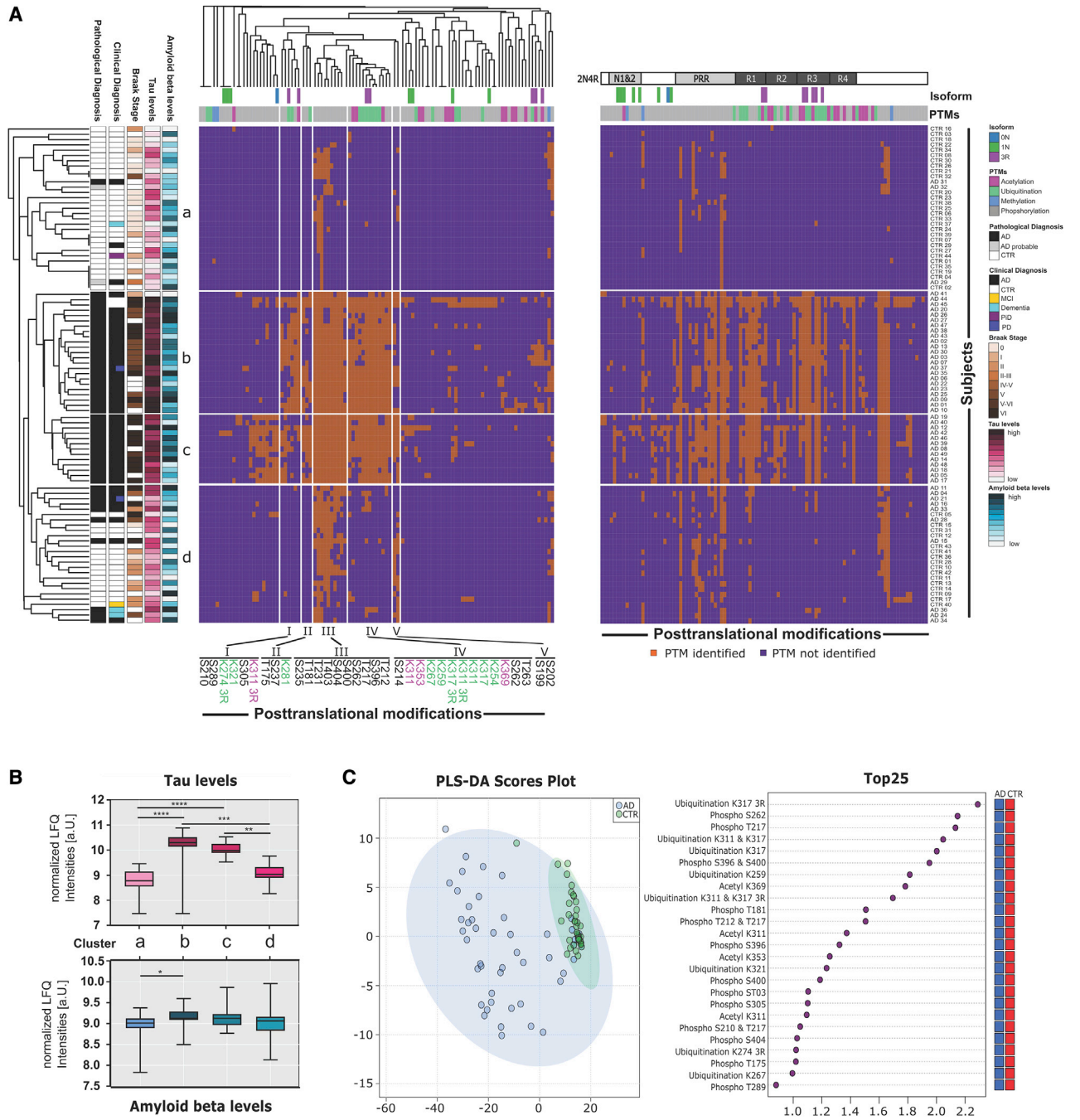

Figure 2. The PTM Landscape of Insoluble Tau Is Heterogenous and Stratifies Subjects into Distinct Groups, Reflecting Disease Progression

(A) The left panel ranks PTMs according to the importance of the PTM in hierarchical clustering, whereas the right heatmap depicts PTMs sorted by their positions on 2N4R Tau. On the right, a legend is provided for isoforms, PTM types, pathological diagnosis, clinical diagnosis [Control (CTR), Mild Cognitive Impairment (MCI) Pick's Disease (PiD), Parkinsons Disease (PD)], and Braak stage. The type of PTM and isoform is color coded in the bar at the top, and the diagnosis is shown on the left. Tau PTM mapping data from shotgun MS from 49 AD patients and 42 age-matched healthy subjects were subjected to an unsupervised hierarchical clustering analysis using Jaccard binary clustering (orange, PTM identified; purple, PTM not identified). The analysis separates subjects into subgroups based on unique Tau PTM signatures comprised of multiple combinations of PTMs for each subgroup. The analysis separates subjects into 4 groups (**a**, **b**, **c**, and **d**), with **c** being the group with the highest Braak stage patients and **a** those with the lowest Braak stages. Below the left panel, we list 5 combinations of PTMs that separate the clusters into the 4 groups.

(legend continued on next page)

Please cite this article in press as: Wesseling et al., Tau PTM Profiles Identify Patient Heterogeneity and Stages of Alzheimer's Disease, Cell (2020), https://doi.org/10.1016/j.cell.2020.10.029

differentiating between AD and control groups. This ranks the singly and doubly ubiquitinated peptides at residues K311 and K317 as well as two phosphopeptides (T217 and S262) as the most distinct when differentiating between AD and control groups using quantitative data from post-translationally modified peptides.

Interestingly, the soluble fraction of Tau was also studied using qualitative and quantitative MS, and the PTM maps from AD and control subjects show no differences with respect to the identity and quantity of detected PTMs in the soluble fractions (Figure S3). This observation is consistent with the suggestion that PTMs associated with the soluble fraction are associated with normal physiological Tau function. Although the top-ranked PTMs identified by the PLS-DA in the insoluble fraction, including the ubiquitinated peptides at residue K311 and K317, may be possible biomarkers for diagnosis, an appropriately powered study with relevant biofluid specimens is required.

Tau Peptide Stoichiometry Data Identify Key Pathological Features in Disease

The FLEXITau data for individual patients of the two cohorts are presented in Figure 3 (see Figure S4 for cohort 2 and Figure S2D for BA46). Hierarchical cluster analyses of FLEXITau data are shown as heatmaps, with the highest extent of modifications shown in red and the lowest in blue. On the left, we performed performed hierarchical clustering of peptides, indicating peptides that distinguish between clusters, and the extent of modification from the N to the C terminus of Tau is depicted on the right. The Tau PTM modification stoichiometry in AD shown in the heatmap is so distinct from control patients that they separate at the first branch of the hierarchical clusters. One defining feature for AD is the high extent of modification in the PRR spanning from amino acid (aa) 195-224 (peptides 195-209; 212-221/224). In addition, R1–R4 from aa 243–370 is highly enriched in the AD patients (243–254, 260–267, 281/282–290, 299–317, 306–317, and 354–369/370) (Figure 3A; Figure S4), and most of the peptides in this region are highly modified R2–R3 (260–267, 281–290, 282–290, 299–317, and 306–317). The N-specific region is largely underrepresented (45–67, 68–87, and 88–126), as is the C terminus in AD. This signature of enrichment of MBR peptides, a high modification extent in the PRR, and underrepresentation of the N-specific regions and C terminus was replicated in cohort 2 (Figure S4A) and in the BA46 FLEXITau cluster analysis (Figure S2D). We employed PLS-DA to study which variables are most important for separation of the AD and control groups (Figure 3B; Figure S4B). The analysis provides a VIP score that provides a measure of the importance of each peptide when differentiating between AD and control groups (Figure 3B; Figure S4B). This ranks R4 peptide 14 (354–369), PRR peptide 8 (212–221) harboring the S212, S214, S217, and T220 phosphosites, and C-terminal peptide 17 (407–437) as the most distinct when differentiating between AD and control groups (Figure 3B).

A Spearman correlation analysis shows that the PRR and the C terminus peptides are anti-correlated with an increase in abundance of MBD unmodified peptides in both cohorts (Figures 3C and 3D; Figure S4C) because the C terminus and the PRR show a high modification stoichiometry, as reflected by the decrease in abundance of unmodified peptides. This increase in phosphorylation of Tau may be involved in neutralizing the charge in the MBD domain to promote aggregation, and one could invoke a variant of the hairpin model to support this idea (Jeganathan et al., 2006); the PRR and C terminus peptide intensities correlate with each other, supporting this relationship (Figures 3C and 3D; Figure S4C).

A closer examination shows heterogeneity in modification stoichiometry in the AD patients and within controls. Although the unmodified C-terminal peptide is found with low abundance in AD compared to all controls, there is a control cluster where the C terminus is completely unmodified (Figure 3A) and the other control cluster shows some processing. Apart from this C terminus peptide, all controls seem to show the same general pattern of peptide stoichiometries; for example, the exon 1 peptide (6–23) shows less modification extent than in all other AD patients, and the PRR is somewhat modified in all controls. This suggests that the modification at the C terminus is an early event during aging and AD pathology and can most likely be attributed to caspase-3 and -6 cleavage at D418 and D421.

Finally, we trained a classifier using stochastic gradient descent (SGD) on the FLEXITau data of cohort 1, which we tested in cohort 2. This classifier was able to predict diagnostic pathology with an accuracy of > 0.92 in both cohorts (Figure 3E).

Identifying PTMs Associated with Seeding Activity in Size-Fractionated Tau

The above results from sarkosyl-insoluble (fibrillized) Tau from AD and control subjects indicate that there is processivity and an order in which PTMs occur in the fibrillization process. To further examine these results and determine the minimum set of PTMs associated with seeding competency using our quantitative and qualitative platform, we examined a series of different species of Tau associated with differing molecular weights and seeding capacities, including size-fractionated Tau from human patients, as described previously (Takeda et al., 2015; Figure 4A). Four different Tau fractions were analyzed: (1) sarkosyl-soluble Tau ("soluble"), (2) MC1-isolated Tau (isolated from soluble fraction by MC1 antibody immunoaffinity columns; Jicha et al., 1999b), (3) soluble low-molecular-weight (LMW) Tau (~50 kDa), and (4) oligomeric high-molecular-weight (HMW) Tau (>120 kDa); the latter two were fractionated by size-exclusion chromatography (Takeda et al., 2015). The data from these four Tau fractions were

(B) ANOVA analysis (Kruskal-Wallis) shows that clusters **b** and **c** have higher Tau and amyloid burdens in the angular gyrus than clusters a and d. This is significant for Tau across all clusters and for Aβ between clusters a and b.

(C) PLS-DA of the modified peptide intensities from MaxQuant separates the subjects according to their pathological diagnosis and identifies 25 peptides to be the most discriminative modified peptides. The VIP plot is provided on the right and ranks these PTMs based on their importance when separating AD from control subjects across the 2 cohorts of patients studied. Red and blue squares show whether a peptide is decreased (red) or increased (blue) in the respective disease groups. (p-value : ****$p < 0.0001$, ***$p < 0.001$, **$p < 0.01$, *$p < 0.1$).

Please cite this article in press as: Wesseling et al., Tau PTM Profiles Identify Patient Heterogeneity and Stages of Alzheimer's Disease, Cell (2020), https://doi.org/10.1016/j.cell.2020.10.029

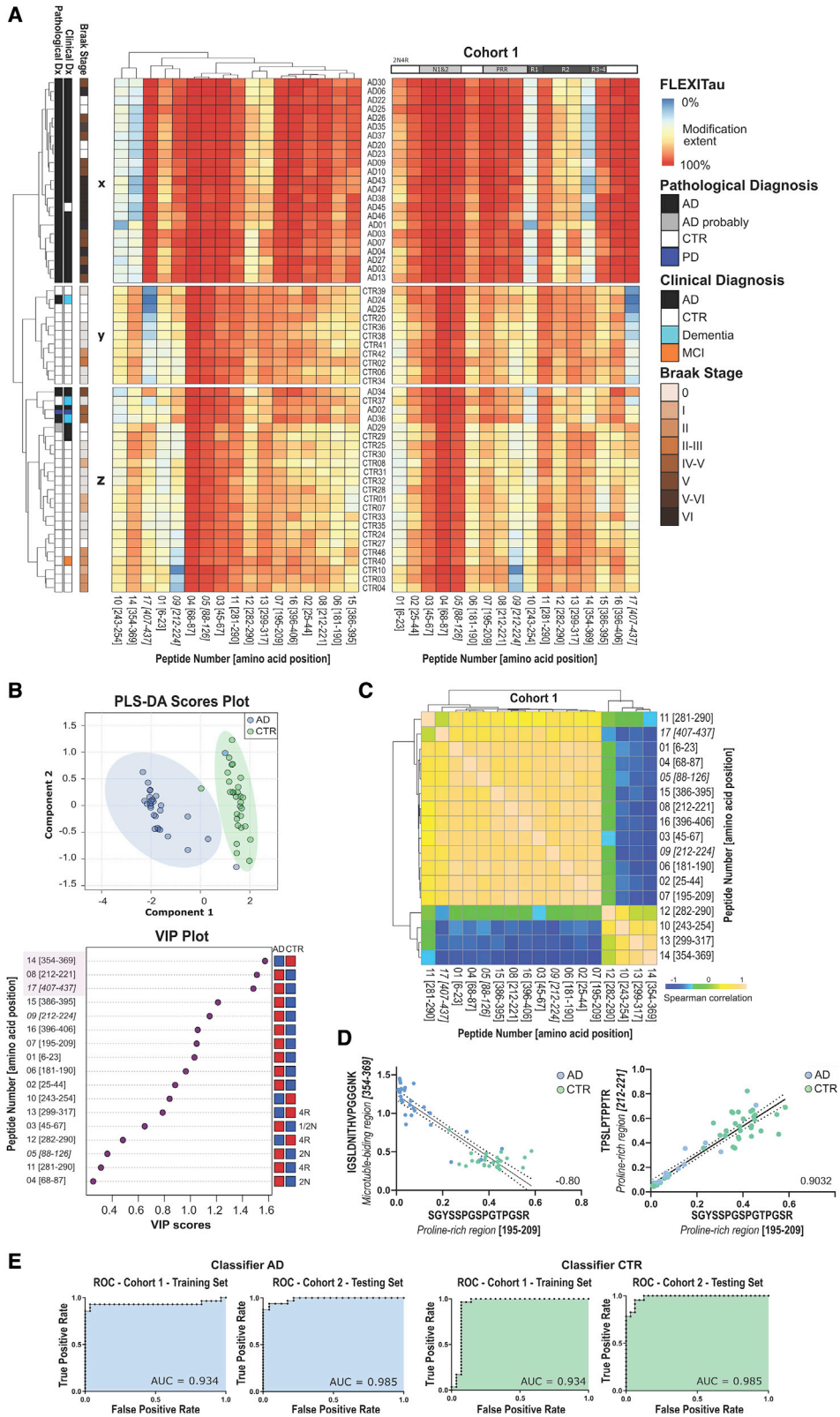

(legend on next page)

Please cite this article in press as: Wesseling et al., Tau PTM Profiles Identify Patient Heterogeneity and Stages of Alzheimer's Disease, Cell (2020), https://doi.org/10.1016/j.cell.2020.10.029

compared with the data from our insoluble Tau isolates (fibrillar Tau, "insoluble").

To better understand the molecular nature of the Tau species in each fraction, we compared the relative peptide quantities of the measured species (Figure 4B; Figure S2B). When we compare the Tau profiles of the LMW and HMW Tau species in the top left panel, we see that the unmodified intrinsically disordered domain encompassing the N terminus to the end of the PRR is overrepresented in LMW Tau, which is seeding incompetent in the biosensor assay (Takeda et al., 2015), whereas the modified MBD is overrepresented in the HMW Tau seeding-competent fraction. When the sarkosyl-insoluble fraction of AD (seeding competent) and control (seeding incompetent) subjects is compared in this manner, we obtain a similar result. Comparative analysis of the two seeding-competent fractions, HMW Tau and the larger, fibrillized, insoluble Tau, shows a similar pattern; however, the MBD is even more enriched in the insoluble Tau fraction, and the peptide 260–267 is underrepresented, indicating a higher phosphorylation stoichiometry of this peptide (S262 and T263). The PTM extent of Tau peptides in each of the five fractions is shown in Figure 4C. The seeding-incompetent AD and control Tau sarkosyl-soluble fractions show no differences; both are enriched in the N-terminal regions (Figure 4C). These quantitative data suggest that the N-terminal region of Tau is negatively correlated with seeding capacity. In contrast, a high concentration of MBD is positively correlated with seeding activity and fibril size. In Figure 4D, the modification profiles of the 5 described Tau species are mapped. LMW Tau shows a similar modification pattern to Tau as the sarkosyl-soluble fraction, with 5 phosphorylations (T181, S198, S199, S202, and T231) in the PRR being consistently observed sites in LMW and sarkosyl-soluble fractions. These Tau fractions do not have positive seeding activity in biosensor assays (Holmes et al., 2014; Takeda et al., 2015). HMW Tau, which is thought to be oligomeric Tau, displays 20 phosphosites (6 in the N terminus, 10 in the PRR, and 4 in the C-terminal region) as well as 3 acetylation and 4 ubiquitin sites in the MBD. In accordance with the observations in other fractions, there is some patient-to-patient variability in the exact patterns of PTMs in the HMW fraction in the context of overall similarities in Tau molecules isolated with these techniques. This HMW oligomeric Tau form appears to have the minimum set of Tau PTMs associated with seeding; we observe acetylation and ubiquitination as being unique to seeding-positive Tau compared with LMW and sarkosyl-soluble seeding-negative fractions. A striking aspect of these modification maps that is consistent with our analysis of sarkosyl-insoluble Tau (Figures 1, 2, and 3) is the fact that the PRR appears to accumulate phosphosites and the MBD appears to accumulate acetylation and ubiquitination with increasing size of Tau aggregates. Interestingly, charge-neutralizing PTMs, such as acetylation and ubiquitination, are mainly found within the core pocket (345–375) of Tau (K353, K369, and K370). Disorder prediction and charge calculations reveal that the MBD becomes neutralized and particularly disordered from residues 305–350 (Figure S5).

Stoichiometric PTM Maps of Human Pathologic Tau Identify Critical Steps in Disease Progression

As a summary of the multiple analyses performed, in Figures 5A and 5B we depict the most salient features observed in the qualitative and quantitative MS data from pathologic Tau.

In Figure 5A, we depict the processive nature of the Tau PTM profiles suggested by the hierarchical clustering analysis. These data indicate that there is an increase in the number of PTMs and the occupancy of these PTM sites observed at different stages of disease, and these provide insights into the aggregation process and disease progression. Cluster a, with the lowest average Braak stage of 0–I, only displayed phosphorylation of Tau (BA39), with 3 sites occupied in the PRR and another 3 in aa 400–404. In cluster d, subjects with an average Braak stage of III–IV, we observed an increase of 6 additional phosphosites in the PRR domain and one in the C terminus at S396. In cluster b, with an average Braak stage of V or VI, we observe the appearance of acetylation and ubiquitination at multiple sites in the MBD. In cluster c, with the highest Braak stage of VI, we observe an overall increase in PTMs from the N to the C terminus.

In Figure 5B, we summarize the FLEXITau analysis results. In general, the qualitative data agree with the quantitative data from the FLEXITau analyses. However, there are interesting observations when comparing the FLEXITau data and the PTM mapping data. The FLEXITau data are important because they identify regions of Tau associated with pathology; for example, the three peptides identified as defining AD are the MBD domain, which is increased in AD subjects; the PRR, which is highly modified in disease; and the endmost C terminus peptide, which is

Figure 3. FLEXITau Analysis of AD Patients and Age-Matched Controls Show Heterogeneity in Quantitative Modification Profiles

(A) FLEXITau provides a measure of the extent of modification of peptides in Tau. The left panel ranks the extent of modification for each measured peptide according to the importance of the peptide in hierarchical clustering, whereas the right heatmap depicts the peptides sorted by their position on 2N4R Tau. On the right, a legend is provided for the extent of modification of each peptide, pathological diagnosis, clinical diagnosis, and Braak stage for the cohort 1 subjects (Table S1). Unsupervised Euclidian hierarchical clustering of Tau peptides was measured using FLEXITau in cohort 1 (29 AD versus 28 CTR subjects). The FLEXITau clustering analysis separates the subjects into 3 major groups (x, y, and z), with the most distinctive features being the stoichiometry of the C terminus peptide, R3–R4 in the MBD, and the PRR.

(B) PLS-DA of the FLEXITau peptide modification extent separates the subjects according to their pathological diagnosis and identifies three peptides to be most discriminative (VIP score plot). Red and blue squares show whether a peptide is decreased (red) or increased (blue) in the respective disease groups.

(C) Spearman correlation analysis shows that the PRR and 1N/2N-specific peptides are anti-correlated, with an increase abundance in the MBD in both cohorts.

(D) Correlation plots of the correlating and anti-correlating peptides in cohort 1. The FLEXITau data reveal an increase in PTM extent in the PRR and C terminus and enrichment of the MBD in AD insoluble aggregates and provides information regarding the processivity of modifications. A similar analysis for cohort 2 is provided in Figure S4.

(E) Receiver operating characteristic (ROC) curves visualizing the classification performance of a 10-fold cross-validated SGD model for predicting AD and control based on FLEXITau data. The model was trained on cohort 1 and tested on cohort 2, which resulted in an AUC of 0.934 and 0.985 for AD and control, respectively. [Diagnosis (Dx)].

Please cite this article in press as: Wesseling et al., Tau PTM Profiles Identify Patient Heterogeneity and Stages of Alzheimer's Disease, Cell (2020), https://doi.org/10.1016/j.cell.2020.10.029

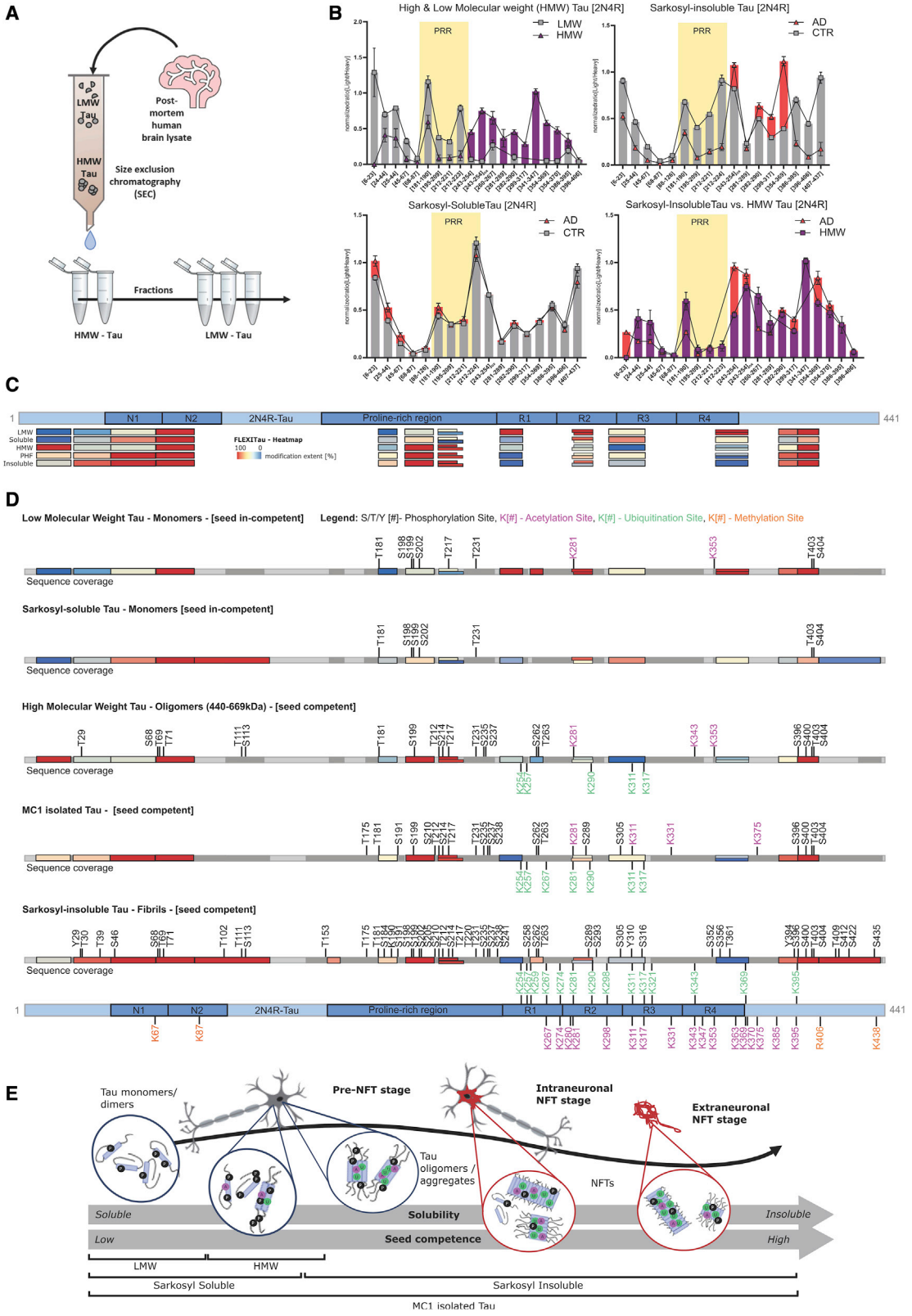

(legend on next page)

Please cite this article in press as: Wesseling et al., Tau PTM Profiles Identify Patient Heterogeneity and Stages of Alzheimer's Disease, Cell (2020), https://doi.org/10.1016/j.cell.2020.10.029

underrepresented in its unmodified form and can be explained by caspase cleavage.

In Figure 5C, we posit a model for Tau fibril formation in AD. Our analyses reveal that the 0N and 4R isoforms are predisposed to aggregation. Furthermore, a stepwise cascade of PTMs, including C terminus cleavage and negatively charged phosphorylation in the PRR, followed by charge-neutralizing acetylation and ubiquitination in the enriched MBR, are progressive steps in the process of Tau fibril formation and AD disease progression.

DISCUSSION

Understanding the Tau proteoforms prevalent in AD pathology and seeding activity is important, particularly because pharmaceutical efforts are pivoting to Tau as a therapeutic target using antibodies and small molecules. Because only ~0.1% of all antibodies can cross the blood-brain barrier (BBB), increasing the specificity and affinity of the intended therapeutic antibody for the pathologic form of Tau is essential for successful therapy (Sigurdsson, 2018). Our analyses provide an unprecedented quantitative and qualitative view of the molecular features of the pathologic Tau species in human disease, which is crucial for rational design of antibody and small-molecule therapeutic agents and diagnostics for Tau. For example, our data show that unmodified exons 1, 2, and 3 peptides spanning the N-terminal region, including the 1N and 2N regions, are underrepresented (>50%) so that an N terminus antibody for this region is predicted to be a less effective therapeutic agent for AD. In addition, an N terminus antibody for the unmodified 1N/2N region may not be as effective at halting disease progression via the seeding mechanism, given that unmodified 1N/2N regions are found to be low in prion-like, seeding-positive Tau aggregates and oligomeric seeds.

Our analysis of pathological Tau from 91 subjects (49 AD and 42 control subjects) cumulatively identifies 95 PTMs at 88 aa residues. We mapped 55 phosphosites, 17 ubiquitination sites, 19 acetylation sites, and four methylation sites along the length of the Tau protein. (Figure 1E). The PTM maps reveal an extensive interplay of distinct PTMs at the same amino acid residues (Figure 1E), an observation partially consistent with recent Tau PTM mapping results in mice (Morris et al., 2015; Table S5). Interestingly, the PTM profiles of pathologic Tau isolated from human brain tissues were heterogeneous across subjects. However, analysis of the frequency of each PTM across the AD and control groups showed a striking pattern, identifying common features in AD. Phosphorylation is observed with highest frequency in the PRR and the C terminus tail, whereas acetylation and ubiquitination cluster heavily in the MBD, which has been shown to form the core region of the Tau filaments (Fitzpatrick et al., 2017). Consistent with previous biochemical studies in mice (Morris et al., 2015; Yang and Seto, 2008), most of the human Tau acetylation sites identified were ubiquitinated alternatively (Figure 1E). These sites include three KXGS motifs, which are known to regulate neurite extension and binding of Tau to microtubules (Biernat et al., 1993; Biernat and Mandelkow, 1999). Well-studied epitopes known to be important in AD, such as AT8 and AT180, were identified in both cohorts with high frequency. Importantly, our data also identified other, less-studied epitopes with equally high frequencies, including ubiquitination at K311 and K317 and acetylation at K369. Unsupervised analyses based on the presence or absence of PTMs clustered the subjects into 4 major groups and revealed that there were specific combinations of PTMs in each of these groups. The sets of PTMs were largely reflective of disease progression and therefore could be associated with disease stages. Importantly, these data suggest that early intervention may need different therapeutic agents than late-stage AD because there are distinct differences in PTM profiles associated with each stage of disease. Exploring the roles of these PTMs may provide mechanistic insights into disease pathology and progression. Furthermore, our data provide a comprehensive PTM atlas for pathological Tau in human tissue and will be useful for future biomarker studies of systemic and proximal body fluids, such as cerebrospinal fluid (CSF), peripheral mononuclear blood cells (PBMC), platelets, and blood for diagnosis and will facilitate ongoing diagnostic research.

Analysis of size-fractionated seed-competent and -incompetent Tau species isolated from AD patients and control subjects reveals that the Tau PTM landscape, as shown in Figure 4, differs between seeding-competent (HMW and sarkosyl-insoluble Tau) and non-seeding-competent Tau species (LMW and sarkosyl-soluble Tau). We identify the minimal set of PTMs associated with prion-like activity, and our data suggest that these modifications could define novel epitopes to be targeted by therapeutic antibodies to abrogate the spread of disease. Furthermore, the PTM landscape of these different Tau species provides evidence that there is progressive accumulation of PTMs as the size of the Tau species increases gradually from LMW Tau, HMW Tau, and MC1-purified Tau to sarkosyl-insoluble fibrillar Tau. PTMs identified in MC1-purified Tau were largely identical to those in AD fibrillar Tau from the sarkosyl-insoluble fraction. These data, in conjunction with seeding competence studies, provides the minimal set of PTMs required to form an oligomer, as mapped on HMW Tau. Although acetylation and ubiquitination are observed in the MBD of HMW Tau, the latter modification appears to be exclusive to seeding-

Figure 4. Identifying PTMs Associated with Seeding Activity in Size-Fractionated Tau

A) A schematic of the workflow used to isolate soluble fractions of size-separated, seeding-competent HMW Tau oligomers and seeding-incompetent LMW Tau.

(B) Comparative analysis of FLEXITau-quantified peptides listed from the N and C termini in the different fractions.

(C) Median peptide modification extent calculated from quantitative FLEXITau assays obtained by targeted MS experiments.

(D) Cumulative PTM maps of seeding-competent and -incompetent Tau separated by size: LMW Tau, sarkosyl-soluble Tau, oligomeric Tau (HMW), MC1-isolated Tau, and the sarkosyl-insoluble fraction containing fibrillar Tau. HMW and LMW Tau fractions were isolated by size-exclusion chromatography from the cortex of 4 control subjects and 4 AD patients. LMW Tau and soluble Tau exhibit 9 PTMs, HMW Tau oligomers exhibit 26 PTMs, and a cumulative map from sarkosyl-insoluble fibrillar Tau displays 85 PTMs.

(E) A schematic representation showing the size differences of Tau species from various fractions: sarkosyl-soluble, LMW, HMW, MC1 antibody isolates, and sarkosyl-insoluble. [# represents amino acid position in 2N4R Tau].

Please cite this article in press as: Wesseling et al., Tau PTM Profiles Identify Patient Heterogeneity and Stages of Alzheimer's Disease, Cell (2020), https://doi.org/10.1016/j.cell.2020.10.029

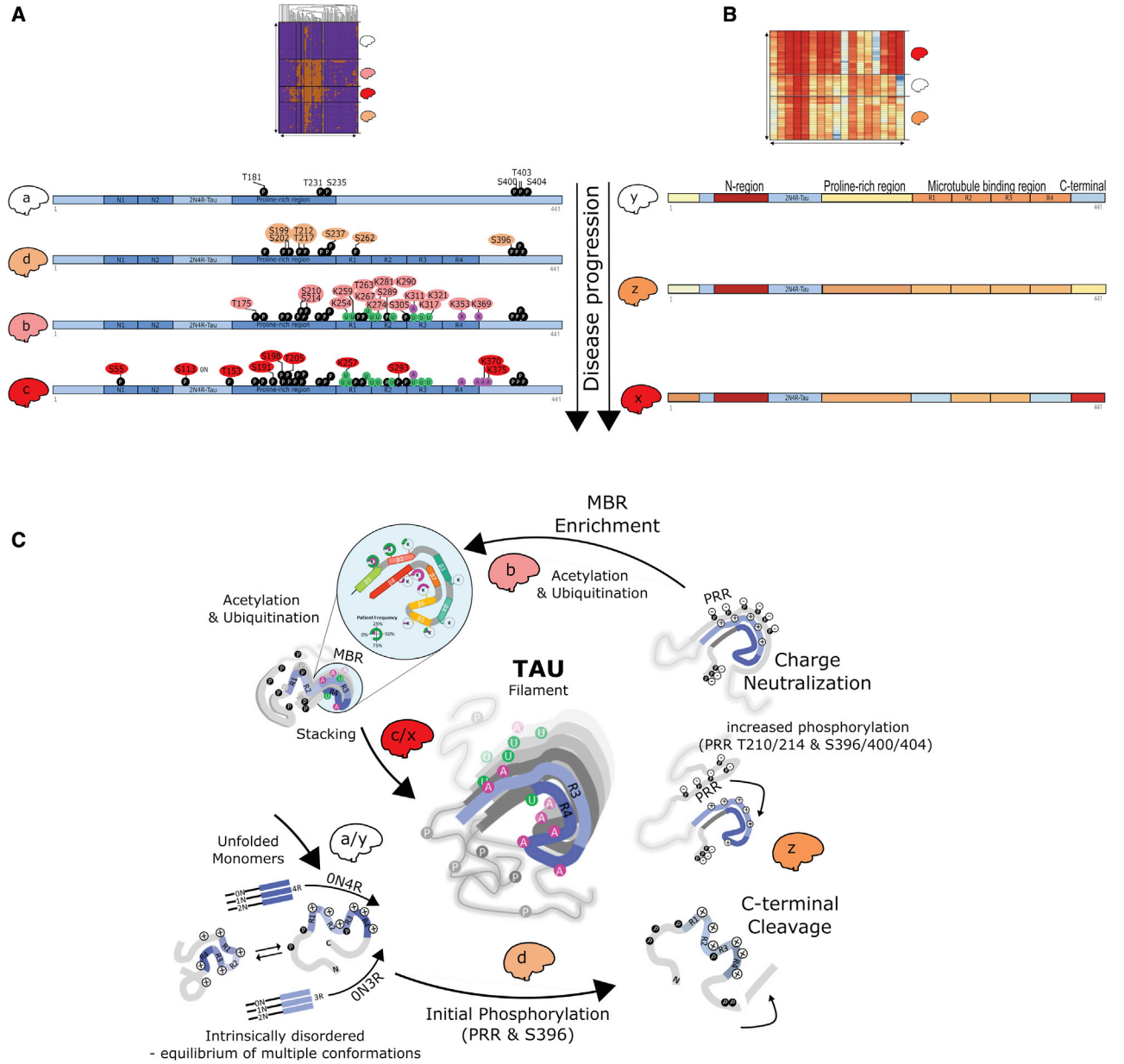

Figure 5. Comparative Stoichiometric Tau PTM Maps in Disease and Control Patients Identify Critical PTMs and Regions Associated with Aggregation

(A) Schematic representation of sequential accumulation of different PTMs at different stages of disease. Increased phosphorylation in the PRR is followed by acetylation and ubiquitination in the MBD as the disease progresses.

(B) Schematic summarizing the FLEXITau data, showing a three-step process that leads to Tau aggregation across patients. The 1N and 2N isoforms are underrepresented in all insoluble Tau. An early event that is observed is cleavage of the C terminus, and this is followed by phosphorylation of the PRR and enrichment of the MBD. Enrichment of the MBD is notable in AD patients compared to control.

(C) Based on our stoichiometric PTM analysis, we posit a model for Tau fibril formation. The 0N and 4R isoforms are predisposed to aggregation. A cascade of PTMs, including C terminus cleavage, negatively charged phosphorylation in the PRR, followed by charge-neutralizing acetylation and ubiquitination in the enriched MBR are progressive steps in the process of Tau fibril formation and AD disease progression.

competent species. Ubiquitination is unique to seeding-competent Tau, whereas acetylation is also observed in seeding-incompetent Tau. Tau has 19 lysine residues in the MBD, which would be charged positively at physiological pH and experience repulsive electrostatic forces, preventing formation of a β sheet fibril structure. To overcome these electrostatic forces and promote aggregation, charge neutralization of the MBD is required, and anionic experimental cofactor models have been described to promote aggregation: heparin (Goedert et al., 1996; Fichou et al., 2018) and RNA or its associated granules (Kampers et al., 1996; Zhang

et al., 2017; Dinkel et al., 2015). Our data suggest that multiple PTMs could contribute to charge neutralization of the MBD, including phosphorylation, acetylation, and ubiquitination. Increased phosphorylation in the PRR results in accumulation of negative charges, which, we postulate, could neutralize the positive charge in the MBD, much like heparin neutralizes the positive charge of this region to induce Tau fibrillization. We also observe that the MBD accumulates charge-neutralizing PTMs such as acetylation and ubiquitination. Charge-neutralizing PTMs at K311, K317, K321, and K369 ubiquitination/acetylation would reduce kinetic barriers to filament formation. Moreover, the increase in these modifications correlates positively with increasing polymer length and increased abundance of pathological Tau associated with disease progression. The patient frequency of these PTMs is high; however, the stoichiometry of these sites is ~50%; thus, every second Tau molecule in a fibril is modified. These data indicate that not every Tau molecule at the described sites in the fibril is acetylated or ubiquitinated.

The disordered regions of Tau span the N terminus and PRR. Our quantitative analyses of different Tau isoforms show that the 4R isoform dominates aggregates and that the 2N and 1N regions are negatively correlated with the abundance of seeding-competent pathological Tau, whereas phosphorylation in the PRR is highly correlated with pathology. These data suggest that the 0N and 4R version, when phosphorylated, is no longer disordered and can adopt a structure capable of fibril formation. Thus, an alternate pathway toward fibril formation is one that involves the highly phosphorylated, negatively charged PRR domain neutralizing positive charges of the MBD lysines by folding back on the MBD in a modified version of the previously described hairpin structure (Jeganathan et al., 2006), where the phosphorylated C terminus and phosphorylated PRR domain stabilize the positive charge of the MBD.

Our data support a processive model (Figure 5C) where 0N and 4R are predisposed to aggregation with initial phosphorylation, cleavage of the C terminus enables further fibrillization, followed by increased phosphorylation in the PRR domain and acetylation and ubiquitination in the MBD, which remove electrostatic repulsion of positively charged lysine residues in this region, promoting Tau fibrillization. These data provide a guide for diagnostic criteria and therapeutic strategies for each stage of disease; for example, antibodies or small-molecule therapeutic agents specific to each stage of disease in AD need to be developed. Overall, MS is a powerful tool for understanding the mechanisms of Tau aggregation and may enable future *in vivo* diagnostic and prognostic tools as well as therapeutic approaches.

STAR★METHODS

Detailed methods are provided in the online version of this paper and include the following:

- KEY RESOURCES TABLE
- RESOURCE AVAILABILITY
  - Lead Contact
  - Materials Availability
  - Data and Code Availability
- EXPERIMENTAL MODEL AND SUBJECT DETAILS
- METHOD DETAILS
  - Preparation of brain tissue samples and mass spectrometry (MS) analysis
  - Preparation of high and low molecular weight Tau and mass spectrometric analysis
  - Preparation and MS analysis of MC1-isolated Tau
- QUANTIFICATION AND STATISTICAL ANALYSIS

SUPPLEMENTAL INFORMATION

Supplemental Information can be found online at https://doi.org/10.1016/j.cell.2020.10.029.

ACKNOWLEDGMENTS

This study was funded by the Tau Consortium (TC). We are grateful to the Rainwater family, Todd, Matt, Lowisa and Jessie, for their interest and support of tauopathy research. We thank the TC directors and staff: Jeremy Smith, Patrick Brannelly, Amy Rommel, Leticia Toledo-Sherman, and Beth Taylor. We are grateful to the SAB members Jim Audia, Patrick May, Howard Feldman, Eric Nestler, Hui Zheng, Maria Spillantini, and Bradley Boeve and the TC scientific community for insightful comments and support of the work in this manuscript. The instruments, software, and infrastructure used for this work were funded by National Institutes of Health grants R01 GM112007, RC4GM096319 (QTRAP 5500, to H.S.), and R01 NS066973 (Q Exactive, to J.A.S.). Tissues were from the NIH NeuroBioBank, the Human Brain and Spinal Fluid Resource Center (VA West LA Healthcare Center funded by NINDS/NIMH, National Multiple Sclerosis Society, and the US Department of Veterans Affairs), the University of Maryland Brain and Tissue Bank, the University of Miami Brain Endowment Bank (HHS-NIH-NIDA(MH)-12-265 and the Francis and Norris McGowan Endowment Fund), the Harvard Brain Tissue Resource Center (HHSN-271-2013-00030C), and the Neurodegenerative Disease Brain Bank at UCSF (TC, Consortium for FTD Research, and NIA AG023501 and AG19724). We thank Rudolph Castellani (neuropathological evaluation), Deborah C. Mash, James S. Riehl, and John Cottrell (technical support).

AUTHOR CONTRIBUTIONS

Conceptualization, J.A.S.; Methodology, J.A.S., H.S., W.M., H.W., B.F., and J.M.; Validation, H.W., W.M., M.K., M.S.R., S.T., S.D., W.W.S., L.T.G., J.C.H., S.B., and P.D.; Formal Analysis, H.W., W.M., C.N.S., J.A.S., H.S., and S.T.; Investigation, H.W., W.M., A.J.G., P.B., and M.K.; Resources, J.A.S., H.S., K.S.K., B.L.M., W.W.S., L.T.G., J.C.H., and S.B.; Data Curation, H.W., W.M., C.N.S., and M.K.; Writing – Original Draft, J.A.S.; Writing – Review & Editing, J.A.S., H.S., H.W., W.M., M.K., C.N.S., L.C., P.B., A.J.G., S.T., B.F., J.M., M.S.R., K.S.K., B.L.M., B.T.H., W.W.S., L.T.G., J.C.H., S.B., P.D., and S.D.; Visualization, H.W., J.A.S., H.S., and L.C.; Supervision, J.A.S.; Project Administration, J.A.S.; Funding Acquisition, J.A.S.

DECLARATION OF INTERESTS

B.T.H. is a member of the SAB and owns shares in Dewpoint. He also serves on an advisory panel for Biogen, and his laboratory has current research funding from AbbVie. His wife is an employee and shareholder of Novartis.

Received: March 3, 2020
Revised: August 27, 2020
Accepted: October 16, 2020
Published: November 13, 2020

REFERENCES

Abreha, M.H., Dammer, E.B., Ping, L., Zhang, T., Duong, D.M., Gearing, M., Lah, J.J., Levey, A.I., and Seyfried, N.T. (2018). Quantitative Analysis of the Brain Ubiquitylome in Alzheimer's Disease. Proteomics *18*, e1800108.

Adams, S.J., DeTure, M.A., McBride, M., Dickson, D.W., and Petrucelli, L. (2010). Three repeat isoforms of tau inhibit assembly of four repeat tau filaments. PLoS ONE *5*, e10810.

Aebersold, R., Agar, J.N., Amster, I.J., Baker, M.S., Bertozzi, C.R., Boja, E.S., Costello, C.E., Cravatt, B.F., Fenselau, C., Garcia, B.A., et al. (2018). How many human proteoforms are there? Nat. Chem. Biol. *14*, 206–214.

Alonso, A., Zaidi, T., Novak, M., Grundke-Iqbal, I., and Iqbal, K. (2001). Hyperphosphorylation induces self-assembly of tau into tangles of paired helical filaments/straight filaments. Proc. Natl. Acad. Sci. USA *98*, 6923–6928.

Arendt, T., Stieler, J.T., and Holzer, M. (2016). Tau and tauopathies. Brain Res. Bull. *126*, 238–292.

Arriagada, P.V., Marzloff, K., and Hyman, B.T. (1992). Distribution of Alzheimer-type pathologic changes in nondemented elderly individuals matches the pattern in Alzheimer's disease. Neurology *42*, 1681–1688.

Bierer, L.M., Hof, P.R., Purohit, D.P., Carlin, L., Schmeidler, J., Davis, K.L., and Perl, D.P. (1995). Neocortical neurofibrillary tangles correlate with dementia severity in Alzheimer's disease. Arch. Neurol. *52*, 81–88.

Biernat, J., and Mandelkow, E.M. (1999). The development of cell processes induced by tau protein requires phosphorylation of serine 262 and 356 in the repeat domain and is inhibited by phosphorylation in the proline-rich domains. Mol. Biol. Cell *10*, 727–740.

Biernat, J., Gustke, N., Drewes, G., Mandelkow, E.M., and Mandelkow, E. (1993). Phosphorylation of Ser262 strongly reduces binding of tau to microtubules: distinction between PHF-like immunoreactivity and microtubule binding. Neuron *11*, 153–163.

Braak, H., and Braak, E. (1991). Neuropathological stageing of Alzheimer-related changes. Acta Neuropathol. *82*, 239–259.

Bramblett, G.T., Goedert, M., Jakes, R., Merrick, S.E., Trojanowski, J.Q., and Lee, V.M. (1993). Abnormal tau phosphorylation at Ser396 in Alzheimer's disease recapitulates development and contributes to reduced microtubule binding. Neuron *10*, 1089–1099.

Brosch, J.R., Farlow, M.R., Risacher, S.L., and Apostolova, L.G. (2017). Tau Imaging in Alzheimer's Disease Diagnosis and Clinical Trials. Neurotherapeutics *14*, 62–68.

Clavaguera, F., Lavenir, I., Falcon, B., Frank, S., Goedert, M., and Tolnay, M. (2013). "Prion-like" templated misfolding in tauopathies. Brain Pathol. *23*, 342–349.

Cleveland, D.W., Hwo, S.Y., and Kirschner, M.W. (1977). Physical and chemical properties of purified tau factor and the role of tau in microtubule assembly. J. Mol. Biol. *116*, 227–247.

Cohen, T.J., Guo, J.L., Hurtado, D.E., Kwong, L.K., Mills, I.P., Trojanowski, J.Q., and Lee, V.M. (2011). The acetylation of tau inhibits its function and promotes pathological tau aggregation. Nat. Commun. *2*, 252.

Cox, J., and Mann, M. (2008). MaxQuant enables high peptide identification rates, individualized p.p.b.-range mass accuracies and proteome-wide protein quantification. Nat. Biotechnol. *26*, 1367–1372.

Cox, J., Neuhauser, N., Michalski, A., Scheltema, R.A., Olsen, J.V., and Mann, M. (2011). Andromeda: a peptide search engine integrated into the MaxQuant environment. J. Proteome Res. *10*, 1794–1805.

Cox, J., Hein, M.Y., Luber, C.A., Paron, I., Nagaraj, N., and Mann, M. (2014). Accurate proteome-wide label-free quantification by delayed normalization and maximal peptide ratio extraction, termed MaxLFQ. Mol. Cell. Proteomics *13*, 2513–2526.

Crowther, T., Goedert, M., and Wischik, C.M. (1989). The repeat region of microtubule-associated protein tau forms part of the core of the paired helical filament of Alzheimer's disease. Ann. Med. *21*, 127–132.

de Calignon, A., Polydoro, M., Suárez-Calvet, M., William, C., Adamowicz, D.H., Kopeikina, K.J., Pitstick, R., Sahara, N., Ashe, K.H., Carlson, G.A., et al. (2012). Propagation of tau pathology in a model of early Alzheimer's disease. Neuron *73*, 685–697.

Dinkel, P.D., Holden, M.R., Matin, N., and Margittai, M. (2015). RNA Binds to Tau Fibrils and Sustains Template-Assisted Growth. Biochemistry *54*, 4731–4740.

Escher, C., Reiter, L., MacLean, B., Ossola, R., Herzog, F., Chilton, J., MacCoss, M.J., and Rinner, O. (2012). Using iRT, a normalized retention time for more targeted measurement of peptides. Proteomics *12*, 1111–1121.

Falcon, B., Zhang, W., Schweighauser, M., Murzin, A.G., Vidal, R., Garringer, H.J., Ghetti, B., Scheres, S.H.W., and Goedert, M. (2018). Tau filaments from multiple cases of sporadic and inherited Alzheimer's disease adopt a common fold. Acta Neuropathol. *136*, 699–708.

Fichou, Y., Lin, Y., Rauch, J.N., Vigers, M., Zeng, Z., Srivastava, M., Keller, T.J., Freed, J.H., Kosik, K.S., and Han, S. (2018). Cofactors are essential constituents of stable and seeding-active tau fibrils. Proc. Natl. Acad. Sci. USA *115*, 13234–13239.

Fitzpatrick, A.W.P., Falcon, B., He, S., Murzin, A.G., Murshudov, G., Garringer, H.J., Crowther, R.A., Ghetti, B., Goedert, M., and Scheres, S.H.W. (2017). Cryo-EM structures of tau filaments from Alzheimer's disease. Nature *547*, 185–190.

Giannakopoulos, P., Herrmann, F.R., Bussière, T., Bouras, C., Kövari, E., Perl, D.P., Morrison, J.H., Gold, G., and Hof, P.R. (2003). Tangle and neuron numbers, but not amyloid load, predict cognitive status in Alzheimer's disease. Neurology *60*, 1495–1500.

Glenner, G.G., and Wong, C.W. (1984). Alzheimer's disease: initial report of the purification and characterization of a novel cerebrovascular amyloid protein. Biochem. Biophys. Res. Commun. *120*, 885–890.

Goedert, M., Jakes, R., and Vanmechelen, E. (1995). Monoclonal antibody AT8 recognises tau protein phosphorylated at both serine 202 and threonine 205. Neurosci. Lett. *189*, 167–169.

Goedert, M., Jakes, R., Spillantini, M.G., Hasegawa, M., Smith, M.J., and Crowther, R.A. (1996). Assembly of microtubule-associated protein tau into Alzheimer-like filaments induced by sulphated glycosaminoglycans. Nature *383*, 550–553.

Gómez-Isla, T., Hollister, R., West, H., Mui, S., Growdon, J.H., Petersen, R.C., Parisi, J.E., and Hyman, B.T. (1997). Neuronal loss correlates with but exceeds neurofibrillary tangles in Alzheimer's disease. Ann. Neurol. *41*, 17–24.

Grundke-Iqbal, I., Iqbal, K., Quinlan, M., Tung, Y.C., Zaidi, M.S., and Wisniewski, H.M. (1986). Microtubule-associated protein tau. A component of Alzheimer paired helical filaments. J. Biol. Chem. *261*, 6084–6089.

Guo, T., Noble, W., and Hanger, D.P. (2017). Roles of tau protein in health and disease. Acta Neuropathol. *133*, 665–704.

Hanger, D.P., Byers, H.L., Wray, S., Leung, K.Y., Saxton, M.J., Seereeram, A., Reynolds, C.H., Ward, M.A., and Anderton, B.H. (2007). Novel phosphorylation sites in tau from Alzheimer brain support a role for casein kinase 1 in disease pathogenesis. J. Biol. Chem. *282*, 23645–23654.

Hasegawa, M., Morishima-Kawashima, M., Takio, K., Suzuki, M., Titani, K., and Ihara, Y. (1992). Protein sequence and mass spectrometric analyses of tau in the Alzheimer's disease brain. J. Biol. Chem. *267*, 17047–17054.

Holmes, B.B., Furman, J.L., Mahan, T.E., Yamasaki, T.R., Mirbaha, H., Eades, W.C., Belaygorod, L., Cairns, N.J., Holtzman, D.M., and Diamond, M.I. (2014). Proteopathic tau seeding predicts tauopathy in vivo. Proc. Natl. Acad. Sci. USA *111*, E4376–E4385.

Jackson, S.J., Kerridge, C., Cooper, J., Cavallini, A., Falcon, B., Cella, C.V., Landi, A., Szekeres, P.G., Murray, T.K., Ahmed, Z., et al. (2016). Short Fibrils Constitute the Major Species of Seed-Competent Tau in the Brains of Mice Transgenic for Human P301S Tau. J. Neurosci. *36*, 762–772.

Janelidze, S., Mattsson, N., Palmqvist, S., Smith, R., Beach, T.G., Serrano, G.E., Chai, X., Proctor, N.K., Eichenlaub, U., Zetterberg, H., et al. (2020). Plasma P-tau181 in Alzheimer's disease: relationship to other biomarkers, differential diagnosis, neuropathology and longitudinal progression to Alzheimer's dementia. Nat. Med. *26*, 379–386.

Jeganathan, S., von Bergen, M., Brutlach, H., Steinhoff, H.J., and Mandelkow, E. (2006). Global hairpin folding of tau in solution. Biochemistry *45*, 2283–2293.

Jicha, G.A., O'Donnell, A., Weaver, C., Angeletti, R., and Davies, P. (1999a). Hierarchical phosphorylation of recombinant tau by the paired-helical filament-associated protein kinase is dependent on cyclic AMP-dependent protein kinase. J. Neurochem. *72*, 214–224.

Jicha, G.A., Weaver, C., Lane, E., Vianna, C., Kress, Y., Rockwood, J., and Davies, P. (1999b). cAMP-dependent protein kinase phosphorylations on tau in Alzheimer's disease. J. Neurosci. *19*, 7486–7494.

Jucker, M., and Walker, L.C. (2013). Self-propagation of pathogenic protein aggregates in neurodegenerative diseases. Nature *501*, 45–51.

Kampers, T., Friedhoff, P., Biernat, J., Mandelkow, E.M., and Mandelkow, E. (1996). RNA stimulates aggregation of microtubule-associated protein tau into Alzheimer-like paired helical filaments. FEBS Lett. *399*, 344–349.

Kessner, D., Chambers, M., Burke, R., Agus, D., and Mallick, P. (2008). ProteoWizard: open source software for rapid proteomics tools development. Bioinformatics *24*, 2534–2536.

Kosik, K.S., Joachim, C.L., and Selkoe, D.J. (1986). Microtubule-associated protein tau (tau) is a major antigenic component of paired helical filaments in Alzheimer disease. Proc. Natl. Acad. Sci. USA *83*, 4044–4048.

Lê, S., Josse, J., and Husson, F. (2008). FactoMineR: A Package for Multivariate Analysis. J. Stat. Softw. *25* (1).

Lovestone, S., and Reynolds, C.H. (1997). The phosphorylation of tau: a critical stage in neurodevelopment and neurodegenerative processes. Neuroscience *78*, 309–324.

MacLean, B., Tomazela, D.M., Shulman, N., Chambers, M., Finney, G.L., Frewen, B., Kern, R., Tabb, D.L., Liebler, D.C., and MacCoss, M.J. (2010). Skyline: an open source document editor for creating and analyzing targeted proteomics experiments. Bioinformatics *26*, 966–968.

Mair, W., Muntel, J., Tepper, K., Tang, S., Biernat, J., Seeley, W.W., Kosik, K.S., Mandelkow, E., Steen, H., and Steen, J.A. (2016). FLEXITau: Quantifying Post-translational Modifications of Tau Protein in Vitro and in Human Disease. Anal. Chem. *88*, 3704–3714.

Martin, L., Latypova, X., Wilson, C.M., Magnaudeix, A., Perrin, M.L., and Terro, F. (2013a). Tau protein phosphatases in Alzheimer's disease: the leading role of PP2A. Ageing Res. Rev. *12*, 39–49.

Martin, L., Latypova, X., Wilson, C.M., Magnaudeix, A., Perrin, M.L., Yardin, C., and Terro, F. (2013b). Tau protein kinases: involvement in Alzheimer's disease. Ageing Res. Rev. *12*, 289–309.

Masters, C.L., Simms, G., Weinman, N.A., Multhaup, G., McDonald, B.L., and Beyreuther, K. (1985). Amyloid plaque core protein in Alzheimer disease and Down syndrome. Proc. Natl. Acad. Sci. USA *82*, 4245–4249.

Min, S.W., Cho, S.H., Zhou, Y., Schroeder, S., Haroutunian, V., Seeley, W.W., Huang, E.J., Shen, Y., Masliah, E., Mukherjee, C., et al. (2010). Acetylation of tau inhibits its degradation and contributes to tauopathy. Neuron *67*, 953–966.

Min, S.W., Chen, X., Tracy, T.E., Li, Y., Zhou, Y., Wang, C., Shirakawa, K., Minami, S.S., Defensor, E., Mok, S.A., et al. (2015). Critical role of acetylation in tau-mediated neurodegeneration and cognitive deficits. Nat. Med. *21*, 1154–1162.

Mirra, S.S., Heyman, A., McKeel, D., Sumi, S.M., Crain, B.J., Brownlee, L.M., Vogel, F.S., Hughes, J.P., van Belle, G., and Berg, L. (1991). The Consortium to Establish a Registry for Alzheimer's Disease (CERAD). Part II. Standardization of the neuropathologic assessment of Alzheimer's disease. Neurology *41*, 479–486.

Montine, T.J., Monsell, S.E., Beach, T.G., Bigio, E.H., Bu, Y., Cairns, N.J., Frosch, M., Henriksen, J., Kofler, J., Kukull, W.A., et al. (2016). Multisite assessment of NIA-AA guidelines for the neuropathologic evaluation of Alzheimer's disease. Alzheimers Dement. *12*, 164–169.

Morishima-Kawashima, M., Hasegawa, M., Takio, K., Suzuki, M., Yoshida, H., Titani, K., and Ihara, Y. (1995). Proline-directed and non-proline-directed phosphorylation of PHF-tau. J. Biol. Chem. *270*, 823–829.

Morris, M., Knudsen, G.M., Maeda, S., Trinidad, J.C., Ioanoviciu, A., Burlingame, A.L., and Mucke, L. (2015). Tau post-translational modifications in wild-type and human amyloid precursor protein transgenic mice. Nat. Neurosci. *18*, 1183–1189.

Mudher, A., Colin, M., Dujardin, S., Medina, M., Dewachter, I., Alavi Naini, S.M., Mandelkow, E.M., Mandelkow, E., Buée, L., Goedert, M., and Brion, J.P. (2017). What is the evidence that tau pathology spreads through prion-like propagation? Acta Neuropathol. Commun. *5*, 99.

Poorkaj, P., Bird, T.D., Wijsman, E., Nemens, E., Garruto, R.M., Anderson, L., Andreadis, A., Wiederholt, W.C., Raskind, M., and Schellenberg, G.D. (1998). Tau is a candidate gene for chromosome 17 frontotemporal dementia. Ann. Neurol. *43*, 815–825.

Renard, B.Y., Kirchner, M., Monigatti, F., Ivanov, A.R., Rappsilber, J., Winter, D., Steen, J.A., Hamprecht, F.A., and Steen, H. (2009). When less can yield more - Computational preprocessing of MS/MS spectra for peptide identification. Proteomics *9*, 4978–4984.

Sigurdsson, E.M. (2018). Tau Immunotherapies for Alzheimer's Disease and Related Tauopathies: Progress and Potential Pitfalls. J. Alzheimers Dis. *64* (s1), S555–S565.

Singh, S., Springer, M., Steen, J., Kirschner, M.W., and Steen, H. (2009). FLEXIQuant: a novel tool for the absolute quantification of proteins, and the simultaneous identification and quantification of potentially modified peptides. J. Proteome Res. *8*, 2201–2210.

Singh, S.A., Winter, D., Kirchner, M., Chauhan, R., Ahmed, S., Ozlu, N., Tzur, A., Steen, J.A., and Steen, H. (2014). Co-regulation proteomics reveals substrates and mechanisms of APC/C-dependent degradation. EMBO J. *33*, 385–399.

Smith, L.M., and Kelleher, N.L.; Consortium for Top Down Proteomics (2013). Proteoform: a single term describing protein complexity. Nat. Methods *10*, 186–187.

Soria, P.S., McGary, K.L., and Rokas, A. (2014). Functional divergence for every paralog. Mol. Biol. Evol. *31*, 984–992.

Spillantini, M.G., Murrell, J.R., Goedert, M., Farlow, M.R., Klug, A., and Ghetti, B. (1998). Mutation in the tau gene in familial multiple system tauopathy with presenile dementia. Proc. Natl. Acad. Sci. USA *95*, 7737–7741.

Stacklies, W., Redestig, H., Scholz, M., Walther, D., and Selbig, J. (2007). pcaMethods–a bioconductor package providing PCA methods for incomplete data. Bioinformatics *23*, 1164–1167.

Takeda, S., Wegmann, S., Cho, H., DeVos, S.L., Commins, C., Roe, A.D., Nicholls, S.B., Carlson, G.A., Pitstick, R., Nobuhara, C.K., et al. (2015). Neuronal uptake and propagation of a rare phosphorylated high-molecular-weight tau derived from Alzheimer's disease brain. Nat. Commun. *6*, 8490.

Thévenot, E.A., Roux, A., Xu, Y., Ezan, E., and Junot, C. (2015). Analysis of the Human Adult Urinary Metabolome Variations with Age, Body Mass Index, and Gender by Implementing a Comprehensive Workflow for Univariate and OPLS Statistical Analyses. J. Proteome Res. *14*, 3322–3335.

Thijssen, E.H., La Joie, R., Wolf, A., Strom, A., Wang, P., Iaccarino, L., Bourakova, V., Cobigo, Y., Heuer, H., Spina, S., et al.; Advancing Research and Treatment for Frontotemporal Lobar Degeneration (ARTFL) investigators (2020). Diagnostic value of plasma phosphorylated tau181 in Alzheimer's disease and frontotemporal lobar degeneration. Nat. Med. *26*, 387–397.

Tramutola, A., Sharma, N., Barone, E., Lanzillotta, C., Castellani, A., Iavarone, F., Vincenzoni, F., Castagnola, M., Butterfield, D.A., Gaetani, S., et al. (2018). Proteomic identification of altered protein O-GlcNAcylation in a triple transgenic mouse model of Alzheimer's disease. Biochim. Biophys. Acta Mol. Basis Dis. *1864*, 3309–3321.

Walker, L.C., Diamond, M.I., Duff, K.E., and Hyman, B.T. (2013). Mechanisms of protein seeding in neurodegenerative diseases. JAMA Neurol. *70*, 304–310.

Wang, Y., and Mandelkow, E. (2016). Tau in physiology and pathology. Nat. Rev. Neurosci. *17*, 5–21.

Wiśniewski, J.R., Zougman, A., Nagaraj, N., and Mann, M. (2009). Universal sample preparation method for proteome analysis. Nat. Methods *6*, 359–362.

Wood, J.G., Mirra, S.S., Pollock, N.J., and Binder, L.I. (1986). Neurofibrillary tangles of Alzheimer disease share antigenic determinants with the axonal microtubule-associated protein tau (tau). Proc. Natl. Acad. Sci. USA *83*, 4040–4043.

Yang, X.J., and Seto, E. (2008). Lysine acetylation: codified crosstalk with other posttranslational modifications. Mol. Cell *31*, 449–461.

Zhang, X., Lin, Y., Eschmann, N.A., Zhou, H., Rauch, J.N., Hernandez, I., Guzman, E., Kosik, K.S., and Han, S. (2017). RNA stores tau reversibly in complex coacervates. PLoS Biol. *15*, e2002183.

Please cite this article in press as: Wesseling et al., Tau PTM Profiles Identify Patient Heterogeneity and Stages of Alzheimer's Disease, Cell (2020), https://doi.org/10.1016/j.cell.2020.10.029

STAR★METHODS

KEY RESOURCES TABLE

REAGENT or RESOURCE	SOURCE	IDENTIFIER
Antibodies		
MCI antibody	Pieter Davis Lab	
Biological Samples		
Healthy adult and Alzheimer's Disease brain tissue	Harvard Brain Tissue Resource Center, McLean Hospital, Harvard Medical School, Belmont, MA, Neurodegenerative Disease Brain Bank (NDBB), Memory and Aging Center, University of California, San Francisco (UCSF), CA University of Maryland Brain & Tissue Bank at the University of Maryland School of Medicine, Baltimore, MD Human Brain and Spinal Fluid Resource Center (HBSFRC), VA West Los Angeles Healthcare Center, Los Angeles, CA. University of Miami (UM) Brain Endowment Bank, Miller School of Medicine, Miami, MD	see Experimental Model and Subject Details and Tables S1 and S2
Chemicals, Peptides, and Recombinant Proteins		
Trypsin (sequencing grade modified trypsin)	Promega, Madison,WI	V517
Urea	Sigma-Aldrich	Cat# U1250
Iodoacetamide	Sigma-Aldrich	Cat# I6125
Water	Thermo Fisher Scientific	Cat# W6-4
Acetonitrile	Thermo Fisher Scientific	Cat# A955-4
Formic acid (FA)	Thermo Fisher Scientific	Cat# A117-50
Acrylamide	Sigma-Aldrich	Cat#
Pierce™ Asp-N Protease, MS Grade	Thermo Fisher Scientific	Cat# 90053
Pierce™, Glu-C, MS Grade	Thermo Fisher Scientific	Cat# 90054
Roche cOmplete, EDTA-free	Millipore Sigma	Cat# 11 873 580 001
Roche PhosSTOP	Millipore Sigma	Cat# 04906837001
IRT peptides	Biognosys, Schlieren, CH	Cat# Ki-3003
SENLYFQGDISR (FLEX-peptide)	Sigma Life Science	N/A
Heavy-isotope labeled lysine, arginine and aspartate	Cambridge Isotope Laboratories, Inc.	N/A
Ni-Sepharose High Performance resin GE Healtcare	GE Healtcare	N/A
Critical Commercial Assays		
Pierce™ BCA Protein Assay Kit	Thermo Scientific™	Cat# 23235
Cell-free wheat germ Expression H Kit-NA	Cell-Free Science	CFS-EDX-PLUS
Deposited Data		
Raw and analyzed data	This paper	ProteomeXchange identifiers: PXD020517, PXD020483, PXD020482, PXD020538, PXD020717
Software and Algorithms		
MaxQuant	Cox lab, Max Planck Institute of Biochemistry, Germany	https://www.maxquant.org
Perseus	Cox lab, Max Planck Institute of Biochemistry, Germany	https://maxquant.net/perseus/

(*Continued on next page*)

Please cite this article in press as: Wesseling et al., Tau PTM Profiles Identify Patient Heterogeneity and Stages of Alzheimer's Disease, Cell (2020), https://doi.org/10.1016/j.cell.2020.10.029

Continued

REAGENT or RESOURCE	SOURCE	IDENTIFIER
R version (3.5.2)	R project	https://www.r-project.org/
ProteoWizard		Kessner et al., 2008
Ggplot2 R package	CRAN	https://ggplot2.tidyverse.org/index.html
Limma R package	Bioconductor	https://doi.org/10.18129/B9.bioc.limma
FactorMineR (2.1) R package	Bioconductor	Lê et al., 2008
D3heatmap (0.6.1.2) R package	CRAN	https://github.com/rstudio/d3heatmap
Heatmaply (1.0) R package	CRAN	https://github.com/talgalili/heatmaply/
Pheatmap (1.0.8) R package	CRAN	https://cran.r-project.org/web/packages/pheatmap/index.html
pcaMethods (1.78.0) R package	Bioconductor	Stacklies et al., 2007
Ropls (1.18.1)	Bioconductor	Thévenot et al., 2015
gradDescentR (1.1.1) R package	CRAN	https://github.com/drizzersilverberg/gradDescentR
ProteinPilot™ Software 4.5 Beta	Sciex	N/A
Skyline	MacCoss Lab Software, University of Washington, Seattle, WA.	MacLean et al., 2010
Xcalibur	Thermo Fisher Scientific	Cat# OPTON-30965
Prism 8.132	GraphPad	https://www.graphpad.com/scientific-software/prism/
Inkscape	Inkscape	N/A
Other		
FASP Protein Digestion Kit	Abcam (Expedeon)	Ab270519
Orbitrap Q Exactive Plus	Thermo Fisher Scientific, Bremen	N/A
Orbitrap Q Exactive HF	Thermo Fisher Scientific, Bremen	N/A
Proteocol C18G 200Å 3 μm, 250 mm length X 300 μm ID,	Trajan Scientific and Medical, Australia	N/A
Superdex200-10/300GL columns	GE Healthcare	N/A
AKTA purifier 10	GE Healtcare	N/A
5500 QTRAP	Sciex	N/A
C-18 microspin columns (SEMSS18V)	Nest group	SEM. SS18V
PicoChip column (150 μm x 10 cm Acquity BEH C18 1.7 μm 130 Å, New Objective, Woburn, MA)	New Objective, Woburn, MA, USA	N/A

RESOURCE AVAILABILITY

Lead Contact

Further information and requests for resources and reagents should be directed to and will be fulfilled by the Lead Contact, Judith A. Steen (Judith.steen@childrens.harvard.edu).

Materials Availability

This study did not generate new unique reagents.

Data and Code Availability

Data are available via ProteomeXchange with identifiers PXD020517, PXD020483, PXD020482, PXD020538, PXD020717. No unreported costum computer code or algorithm was used.

EXPERIMENTAL MODEL AND SUBJECT DETAILS

Human *post-mortem* parietal cortex (Brodmann area, BA39 – angular gyrus) and frontal gyrus (BA46) specimens from patients with AD and non-demented age-matched controls were obtained from 5 different brain banks: *1)* the Neurodegenerative Disease Brain

Bank (NDBB), Memory and Aging Center, University of California, San Francisco (UCSF), CA; *2)* the University of Maryland Brain & Tissue Bank at the University of Maryland School of Medicine, Baltimore, MD; *3)* the Harvard Brain Tissue Resource Center, McLean Hospital, Harvard Medical School, Belmont, MA; *4)* the University of Miami (UM) Brain Endowment Bank, Miller School of Medicine, Miami, MD; *5)* the Human Brain and Spinal Fluid Resource Center (HBSFRC), VA West Los Angeles Healthcare Center, Los Angeles, CA. Tissue from brain banks *2)* to *5)* were acquired through the NIH NeuroBioBank (U.S. Department of Health and Human Services, National Institutes of Health). Pathological and clinical information, if available, was de-identified.

For High molecular Weight Tau preparations, frozen brain tissues from the frontal cortex of four patients with AD and four non-demented control subjects were obtained from the Massachusetts Alzheimer's Disease Research Center Brain Bank. The demographic characteristics of the subjects are shown in Table S1. All the study subjects or their next of kin gave informed consent for the brain donation, and the Massachusetts General Hospital Institutional Review Board approved the study protocol. All the AD subjects fulfilled the NIA-Reagan criteria for high likelihood of AD. Demographic details of patients and control individuals are given in Table S1.

METHOD DETAILS

Preparation of brain tissue samples and mass spectrometry (MS) analysis

Preparation of brain tissue samples for MS

While still frozen, 0.25-0.35 g sections of cortical brain specimens were homogenized in 5 volumes lysis buffer (25 mM Tris-HCl buffer, pH 7.4, containing 150 mM NaCl, 10 mM ethylene diamine tetra acetic acid (EDTA), 10 mM EGTA, 1 mM DTT, 10 mM nicotinamide, 2 μM trichostatin A, phosphatase inhibitor cocktail (Sigma), and protease inhibitor cocktail (Roche)), using Precellys® tissue homogenizer. To obtain insoluble Tau fractions, sarkosyl fractionation was performed as previously described (Mair et al., 2016). Therefore, crude brain homogenates were clarified by centrifugation at 11,000 x g for 30 min at 4°C. Part of the crude Tau fraction was treated with sarkosyl (1% final concentration) for 60 min at 4°C and ultracentrifuged at 100,000 g for 2h at 4°C. The supernatant was transferred to a new tube (sarkosyl-soluble fraction). The sarkosyl-insoluble pellet was carefully washed twice with 10 μl ddH_2O, air-dried, and solubilized in 100 μl 50 mM Tris buffer containing 1% SDS, 10 mM nicotinamide, 2 μM trichostatin A, and phosphatase and protease inhibitor cocktail. The protein concentration in the extracts was determined by bicinchoninic acid assay (BCA Protein Assay Kit, Thermo Scientific).

To quantify absolute Tau amounts and determine the extent of Tau PTMs, sarkosyl-insoluble and soluble fractions were processed using the FLEXITau workflow as previously described (Mair et al., 2016). FLEXITau is an MS-based strategy that is based on the addition of a full-length Tau protein standard containing the N-terminally tagged artificial tryptic FLEX-peptide to the biological sample of interest. Light FLEX-peptide is added in predetermined concentration to calculate absolute quantity of endogenous Tau. The relative peptide abundance of light and heavy Tau peptides can be used to infer modification extent of Tau for each peptide. In brief, Tau was *in vitro* transcribed and translated in a cell-free wheat germ expression (WGE) system according to the manufacturer's protocols (Cell Free Sciences, Wheat Germ Expression H Kit-NA) in the presence of heavy isotope (i.e., ^{13}C and ^{15}N) labeled lysine, arginine and aspartate and subsequently purified using Ni-Sepharose beads (Ni-Sepharose High Performance resin, GE Healthcare). Briefly, after a prewash in binding buffer (20 mM phosphate buffer, pH7.5, 500 mM NaCl, 10 mM imidazole) beads were incubated with WGE (ratio 1:4) for 1h rotating head-over-head at 4°C for binding. After removal of the unbound fraction, beads were washed once with 1x volume and 3 times with 10x volume wash buffer (20 mM phosphate buffer, pH7.5, 500 mM NaCl, 10 mM imidazole). Elution of Tau was carried out in three consecutive steps (binding buffer with 100/300/500 mM imidazole, respectively). Success of enrichment was verified by SDS-PAGE and western blot analysis (data not shown). Pooled eluates were stored at −20°C.

Purified heavy Tau standard or sarkosyl-insoluble Tau fractions were diluted with 8 M urea and processed separately using Filter-Aided Sample Preparation (FASP) (FASP Protein Digestion Kit, Expedeon) with DTT as reduction agent and 1% acrylamide for cysteine alkylation. Protein mixtures were digested with 12.5 ng/μl trypsin (sequencing grade modified trypsin, Promega, Madison, WI) overnight at 37°C. Acidified peptides were desalted using C18 extraction plates (Waters). Vacuum-dried peptides were reconstituted in sample buffer (5% formic acid, 5% acetonitrile (ACN)) containing indexed retention time (iRT) peptides (Biognosys)[2] and 50 fmol/μl non-labeled FLEX-peptide SENLYFQGDISR, synthesized by Sigma Life Science, quantified via amino acid analysis of Molecular Biology Core Facilities, Dana Farber Cancer Institute, Boston, MA). Heavy Tau standard peptides were added to insoluble (light) Tau peptides to achieve approximately a 1:1 ratio of Light-to-Heavy (L/H) tau.

FLEXITau measurements and data analysis

LC-SRM measurements of Tau L/H peptide ratios were performed as described previously (Mair et al., 2016). The FLEXITau SRM assay was optimized for the analysis of *post-mortem* tissue, guided by an extensive list of validated transitions generated in-house through LC-MS/MS analysis of sarkosyl-insoluble Tau on a quadrupole Orbitrap tandem mass spectrometer (Q Exactive, Thermo Fisher Scientific). After optimization of the transition list, peptide mixtures were analyzed on a triple quadrupole mass spectrometer (5500 QTRAP, Sciex) using a micro-autosampler AS3 and a nanoflow UPLC pump (both Eksigent/Sciex), using the trap-elute chip system (cHiPLC nanoflex, Eksigent). Briefly, peptides were first loaded onto the trap-chip (200 μm x 75 μm, ChromXP C18-CL 3 μm 120 A, Nano cHiPLC Eksigent) and then separated using a 120 min gradient from 95% buffer A (0.1% (v/v) formic acid in HPLC-H_2O) and 5% buffer B (0.2% (v/v) formic acid in ACN) to 35% buffer B on the analytical column-chip (75 μm x 15 cm, ChromXP C18-CL 3 μm 120 A, Nano cHiPLC Eksigent). The retention time window was set to 5 min and total scan time to 1.2 s, which ensured a

Please cite this article in press as: Wesseling et al., Tau PTM Profiles Identify Patient Heterogeneity and Stages of Alzheimer's Disease, Cell (2020), https://doi.org/10.1016/j.cell.2020.10.029

dwell time over 20 ms per transition. To avoid sample carry-over, blanks were analyzed between every SRM run. To ensure no bias in acquisition, samples were run in randomized order (three technical replicates per sample). SRM data were analyzed and validated in Skyline (version 2.6, MacCoss Lab Software, University of Washington, Seattle, WA) (MacLean et al., 2010). All peptide transitions were evaluated for variability, similarity between y-ion ratios, elution times, and interfering signals by manual analysis. Peak boundaries were manually inspected and reassigned as needed to ensure correct peak detection and accurate integration. Peptides were considered 'quantifiable' if the peptide transitions had a signal-to-noise of > 3 and at least three light and three heavy high-quality SRM transitions were observed. Peptides were kept for further downstream analysis if quantifiable in every patient sample. The final peptide list consisted of 17 Tau peptides. To compensate for differences in mixing ratio, samples were normalized by the L/H ratio of the least modified peptides. To this end, in each sample, the L/H ratio of peak intensities of each peptide was divided by the average of the three Tau peptides with highest ratio in that sample. Absolute abundance of Tau was calculated using the FLEX peptide L/H ratio as described before (Singh et al., 2009). Amounts of insoluble Tau in each patient samples was calculated in the unit of fmol Tau per mg brain wet weight (average of technical replicates).

An updated version of the FLEXITau SRM assay was run for the second cohort and the frontal gyrus (BA46) (Figure 1D). After optimization of transitions using in-house DDA spectral libraries and heavy-isotope labeled Tau standards (STAR Methods), peptide mixtures were analyzed on the same triple quadrupole mass spectrometer (5500 QTRAP, Sciex) which was coupled to an Eksigent micro-autosampler AS2 and a microflow pump (Eksigent, Dublin, CA) as described above but operated under microflow LC conditions. Here, 2 ug of peptides were loaded on a 25 cm column (Proteocol C18G 200Å 3 μm, 250 mm length X 300 μm ID, Trajan Scientific and Medical, Australia) for 3min at 99% A (0.1% (v/v) formic acid in H_20) and 1% B (0.1% (v/v) formic acid in ACN) at a flow rate of 5 μl/min and separated using a 15 minutes linear gradient (1 to 70% B). The retention time window was set to 0.5 s and total scan time to 0.5 s, which ensured a dwell time of 10 ms of each transition pair. The final transition list including the optimal collision energy for each peptide can be found in the supplemental data. For the sample preparation, the FLEXITau standard was added to the sarkosyl-insoluble or soluble lysates in equimolar amounts (Light-to-Heavy (L/H) ratio 1:1) and processed as described above using FASP (FASP Protein Digestion Kit, Expedeon) and digested with 12.5 ng/ul trypsin overnight at 37°C. Vacuum-dried peptides were reconstituted in sample buffer (5% formic acid, 5% acetonitrile (ACN)) containing indexed retention time (iRT) peptides (Biognosys) (Escher et al., 2012) and 10 fmol/μl non-labeled FLEX-peptide and 100 fmol/ul heavy-isotope labeled isoform specific peptides (AEEAGIGDTPSL[+7.1]EDEAA[+4]GHVTQA[+4]R (0N Tau), STPTAEAEEAGIGDTPSL[+7.1]EDEAA[+4]GHVTQA[+4]R (1N Tau), STPTAEDVTAPLVDEGAP[+6]GK (2N Tau), ESPLQTPTEDGSEEP[+6]GSETSDAK (2N & 1N), KLDL[+7.1]SNV[+6]QSK (4R Tau), LDL[+7.1]SNV[+6]QSK (4R Tau), VQIVYKP[+6]V[+6]DLSK (3R Tau), VPGGGSVQIVYKP[+6]V[+6]DLSK. (4R Tau). To ensure no bias in acquisition, samples were run in randomized order. SRM data were analyzed and manually validated in an updated version of Skyline (version 19.08, MacCoss Lab Software, University of Washington, Seattle, WA) (MacLean et al., 2010). All peptide transitions were evaluated for variability, similarity between y-ion ratios, dotp and dotr products, elution times, and interfering signals by manual analysis as described above. Peak boundaries were manually inspected and reassigned as needed to ensure correct peak detection and accurate integration. Peptides were quantified if the peptide transitions had a signal-to-noise of > 3 and at least three light and three heavy high-quality SRM transitions were observed and normalized the same way as described above. For the isoform-specific peptides, the ratios of the heavy isotope labeled peptides were adjusted to the heavy FLEXITau standard by using the corresponding 2N4R FLEXITau peptides HVPGGGSVQIVYKPVDLSK, ESPLQTPTEDGSEEPGSETSDAK, STPTAEDVTAPLVDEGAPGK.

LC-MS/MS measurements and data analysis

Sarkosyl-insoluble samples of 29 AD patients and 28 matched control individuals were analyzed using a QExactive mass spectrometer (Thermo Fisher Scientific, Bremen) coupled to a micro-autosampler AS2 and a nanoflow HPLC pump (Eksigent, Dublin, CA). Peptides were separated using an in-house packed C18 analytical column (Magic C18 particles, 75 μm × 15 cm; AQUA C18/ 3 μm, Michrom Bioresource) by a linear 120 min gradient starting from 95% buffer A (0.1% (v/v) formic acid in HPLC-H2O) and 5% buffer B (0.2% (v/v) formic acid in acetonitrile) to 35% buffer B. A full mass spectrum with resolution of 70,000 (relative to a mass-to-charge (*m/z)* of 200) was acquired in a mass range of 300–1500 *m/z* (AGC target 3 × 10^6, maximum injection time 20 ms). The 10 most intense ions were selected for fragmentation via higher-energy c-trap dissociation (HCD, resolution 17,500, AGC target 2 × 10^5, maximum injection time 250 ms, isolation window 1.6 *m/z*, normalized collision energy 27%). Due to an update in sample numbers a randomized and balanced second and third batch of 32 patient samples and 21 control samples, respectively was prepared and analyzed using a Q Exactive HF and QE mass spectrometer (Thermo Fisher Scientific, Bremen) coupled to a micro-autosampler AS2 and a nanoflow HPLC pump (Eksigent, Dublin, CA). Peptides were loaded on a capflow PicoChip column (150 μm x 10 cm Acquity BEH C18 1.7 μm 130 Å, New Objective, Woburn, MA) with 2 μl/min solvent A. The proteolytic peptides were eluted from the column using 2% solvent B (0.1% FA) in solvent A, which was increase from 2% to 97% at a flowrate of 1 μl /min. The PicoChip containing an emitter for nanospray ionization was kept at 50°C and mounted directly at the inlet to the HF mass spectrometer. The Q Exactive mass spectrometer was operated under the same mode as described above. The HF mass spectrometer was operated in positive DDA top 20 mode with the following MS1 scan settings: *m/z* range 350-1400, resolution 120,000@ *m/z* 400, AGC target $3e^6$, max IT 60ms. MS2 scan settings: resolution 60000 @ *m/z* 400, AGC target $8e^3$, max IT 100ms, isolation window *m/z* 1.6, NCE 27, underfill ration 1% (intensity threshold $1e^4$), charge state exclusion unassigned, 1, > 6, peptide match preferred, exclude isotopes on, dynamic exclusion 40 s. For a more comprehensive PTM mapping a second batch of 23 patient and control samples

additionally underwent GluC and AspN digestion using the same workflow as described above. Samples were digested for 16 h with GluC followed by a 3 h digestion with AspN at 30°C and desalted and analyzed using a Q Exactive HF mass spectrometer with the PicoChip column as described above.

For the BA46 patient cohort, peptides were loaded onto a capflow PicoChip column (150 μm x 10 cm Acquity BEH C18 1.7 μm 130 Å, New Objective, Woburn, MA) with 2 μl/min solvent A. The PicoChip containing an emitter for nanospray inonization was kept at 50°C and mounted directly at the inlet to the QE mass spectrometer. The proteolytic peptides were eluted from the column using 2% solvent B (0.1% FA) in solvent A, which was increased from 2% to 97% at a flowrate of 1 μl /min for 60min. The mass spectrometer was operated in positive DDA top 10 mode with the following MS1 scan settings: mass-to charge (m/z) range 350-1500, resolution 60,000@ m/z 400, AGC target $3e^6$, max IT 20ms. MS2 scan settings: resolution 17500 @ m/z 400, AGC target 2e5, max IT 250ms, isolation window m/z 1.6, NCE 27, underfill ration 1% (intensity threshold 1e4), charge state exclusion unassigned, 1, > 6, peptide match preferred, exclude isotopes on, dynamic exclusion 20 s.

MS raw data was processed using different software for the identification and quantification of post translational modification (PTM) of Tau. QExactive raw files were converted into mgf data format using ProteoWizard (Kessner et al., 2008) The spectra were centroided and filtered using ms2preproc to select the 6 most intense peaks in a 30 Th window (Renard et al., 2009). Collected spectra were searched against a *Homo sapiens* proteome database (downloaded from uniprot.org on 11/01/2017) with ProteinPilot™ Software 4.5 Beta (Paragon Algorithm 4.5.0.0. 1575, Sciex). The following settings were applied: instrument type 'Orbi MS (1-3ppm)'; 'Urea denaturation'; 'thorough' search mode; 'phosphorylation emphasis', 'acetylation emphasis', 'ID focus on biological modifications'. A cutoff of 85% confidence was employed for all modified peptides. In addition, all MS/MS spectra of identified post-translationally modified peptides were subjected to manual verification.

Raw data were additionally analyzed by MaxQuant software version 1.6.1.10 (Cox and Mann, 2008) and peptide list searched against the *Homo sapiens* Uniprot protein sequence database (December 2017, only reviewed entries appended with common laboratory contaminants [cRAP database, 247 entries]) using the Andromeda search engine (Cox et al., 2011). The following settings were applied: trypsin (specificity set as C-terminal to arginine and lysine) with up to two missed cleavages, mass tolerances set to 20 ppm for the first search and 4.5 ppm for the second search. Oxidation of M, acetylation of N-termini, phosphorylation of S, T, Y, acetylation of K, and ubiquitination (GlyGly) were chosen as variable modifications and propionylation of cysteine as static modification. False discovery rate (FDR) was set to 1% on peptide and protein levels with a minimum length of seven amino acids and was determined by searching a reverse database. Peptide identification was performed with an allowed initial precursor mass deviation up to 7 ppm and an allowed fragment mass deviation of 20 ppm. For all other search parameters, the default settings were used. For the Glu-C and Asp-N digested samples settings were set to the respective enzyme with up to three missed cleavages. Label-free quantification was done using the XIC-based in-built label-free quantification (LFQ) algorithm (Cox et al., 2014) integrated into MaxQuant. Data analysis was performed with the Perseus software in the MaxQuant computation platform and in the R statistical computing environment.

Preparation of high and low molecular weight Tau and mass spectrometric analysis

Preparation of high & low molecular weight Tau fractions

High molecular weight Tau was prepared as described in Takeda et al. (2015). 300-500 mg of frontal cortex tissue was homogenized in 5x volumes of cold Phosphate Buffered Saline (PBS), spun at 10,000 g for 10 min at 4°C and the supernatant was used for size-exclusion chromatography. Human brain PBS-soluble extracts were separated by size-exclusion chromatography (SEC) on single Superdex200 10/300GL columns (GE Healthcare) in PBS (Sigma-Aldrich, filtered through a 0.2-μm membrane filter), at a flow rate of 0.5 ml min^{-1}, with an AKTA purifier 10 (GE Healthcare). Each brain extract was diluted with PBS to contain 6,000 ng of human Tau in a final volume of 900 μl, which was filtered through a 0.2-μm membrane filter and then loaded onto an SEC column. Fractions were collected every 1 min (0.5 ml/fraction) from 5.5 mL elution volume (Fraction 2) to 16.5 mL (Fraction 20). Fraction 3 and 4 (containing the high molecular tau) and Fraction 14, 16, 18 (low molecular tau) were collected for MS analysis. The individual fractions separated by SEC were analyzed by ELISA (Tau (total) Human ELISA kit, diluted 1:50 in kit buffer). Four volumes (vol/vol) of cold acetone (20°C) were added to each fraction, followed by vigorous vortex and incubation for 90 min at −20°C. Samples were then centrifuged at 13,000 g for 10 min at 4°C. After carefully aspirating the supernatant, the pellets were resuspended in 105 μL of PBS. Western Blot analysis using Tau13, Tau46, HT7 and DAKO antibodies confirmed that the fraction 3 and 4 are enriched for Tau (data not shown).

The FASP method was carried out as previously described (Wiśniewski et al., 2009) with adjustments as described here:100 μg proteins were denatured and reduced by adding 400 μL 8 M urea supplemented with 200 mM tris (2-carboxyethyl) phosphine (TCEP) for 30 min at 60 °C. Samples were then loaded on a 10kDa MWCO spin filter column (Milipore) and spun 14,000 × g for 15 min at 23 °C. Two wash steps with 200 μL 8 M urea solution were carried out and proteins were alkylated with 100 μL 0.05 M iodoacetamide solution in 8 M urea, shaking at 600 rpm for one minute and incubated in the dark at (23 °C) for 20 min before centrifugation at 14,000 × *g* for 15 min. Two further washes with 8 M urea solution were carried out and subsequently three washes with 100 μl 50 mM ammonium bicarbonate solutions were performed. Protein digestion was performed with sequencing grade trypsin (Promega) at a nominal enzyme to substrate ratio of 1:50. After incubation for 16 h at 600 rpm, the resulting peptides were eluted in two wash steps with 50 μL ABC and a final spin with 50 μL 0.5 M sodium chloride (NaCl). Peptide eluates were acidified

Please cite this article in press as: Wesseling et al., Tau PTM Profiles Identify Patient Heterogeneity and Stages of Alzheimer's Disease, Cell (2020), https://doi.org/10.1016/j.cell.2020.10.029

and desalted using reversed phase C-18 MicroSpin columns (SEMSS18R, Nest Group) and eluted in two fractions (30% Acetonitrile and 50%–70% Acetonitrile fractions). Samples were vacuum dried and frozen at −20 °C prior to LC–MS/MS analysis.

LC-MS/MS analysis of high and low weight molecular Tau

Randomized samples (SEC fractions 2,3,4 and 14,16,18 for 4 AD and 4 control human brain samples) were analyzed in duplicates using a Q Exactive mass spectrometer (Thermo) coupled to a micro-autosampler AS2 and a nanoflow HPLC pump (Eksigent). Peptides were separated using an in-house packed C18 analytical column (Magic C18 particles, 75 μm × 15 cm; AQUA C18/3 μm, Michrom Bioresource) by a linear 120 min gradient starting from 95% buffer A (0.1% (v/v) formic acid in HPLC-H2O) and 5% buffer B (0.2% (v/v) formic acid in acetonitrile) to 35% buffer B. A full mass spectrum with resolution of 70,000 (relative to an *m/z* of 200) was acquired in a mass range of 300–1500 *m/z* (AGC target 3×10^6, maximum injection time 20 ms). The 10 most intense ions were selected for fragmentation via higher-energy c-trap dissociation (HCD, resolution 17,500, AGC target 2×10^5, maximum injection time 250 ms, isolation window 1.6 *m/z*, normalized collision energy 27%). Q Exactive raw files were converted into mgf data format using ProteoWizard. The spectra were centroided and filtered using ms2preproc to select the 6 most intense peaks in a 30 Th window. Collected spectra were searched against a *Homo sapiens* database (uniprot.org on 04/02/2016) with ProteinPilot™ Software 4.5 Beta (Paragon Algorithm 4.5.0.0. 1575, Sciex). The following settings were applied: instrument type 'Orbi MS (1-3ppm)'; 'Urea denaturation'; 'thorough' search mode; 'phosphorylation emphasis', 'acetylation emphasis', 'ID focus on biological modifications'. A cutoff of 85% confidence was employed for all modified peptides. In addition, all MS/MS spectra of identified post-translationally modified peptides were subjected to manual verification. Raw data were analyzed by MaxQuant software version 1.6.1.10 and peptide list searched against the Uniprot protein sequence database (February 2016, only reviewed entries appended with common laboratory contaminants [cRAP database, 247 entries]) using the Andromeda search engine. The following settings were applied: trypsin (specificity set as C-terminal to arginine and lysine) with up to two missed cleavages, mass tolerances set to 20 ppm for the first search and 4.5 ppm for the second search. Oxidation of M, N-terminal acetylation, phosphorylation of STY, Ubiquitination (GlyGly) and acetylation of K were chosen as dynamic modifications and carbamidomethylation of cysteine as static modification. False discovery rate (FDR) was set to 1% on peptide and protein levels with a minimum length of seven amino acids and was determined by searching a reverse database. Peptide identification was performed with an allowed initial precursor mass deviation up to 7 ppm and an allowed fragment mass deviation of 20 ppm. For all other search parameters, the default settings were used.

Preparation and MS analysis of MC1-isolated Tau

MC1-isolated Tau was obtained from Peter Davis, purified from lysate cleared of large particles and aggregates of 4 separate AD patients using MC-1 antibody immunoaffinity columns as previously described (Jicha et al., 1999a). Purified paired helical filament (PHF) Tau was tryptically digested using the FASP method as described above, with the addition of heavy Tau standard peptide spiked in for FLEXITau experiments. Peptide elutes were acidified and desalted using reversed phase C-18 microspin columns (SEMSS18R, Nest Group), vacuum dried and frozen at −20°C prior to LC-MS/MS analysis. For data-dependent acquisition experiments LC-MS/MS analysis, peptides were loaded on a capflow PicoChip column (150 μm x 10 cm Acquity BEH C18 1.7 μm 130 Å, New Objective, Woburn, MA) with 2 μl/min solvent A. The proteolytic peptides were eluted from the column using a 60min gradient starting at 2% solvent B (0.1% FA) in solvent A, which was increased to 35% at a flowrate of 1 μl /min. The PicoChip containing an emitter for nanospray ionization, which was kept at 50°C and mounted directly at the inlet to the HF mass spectrometer. The mass spectrometer was operated in positive DDA top 20 mode with the following MS1 scan settings: mass-to charge (m/z) range 300-1650, resolution 60,000@ m/z 400, AGC target $3e^6$, max IT 20ms. MS2 scan settings: resolution 30000 @ m/z 400, AGC target $1e^5$, max IT 25ms, isolation window m/z 1.4, NCE 27, charge state exclusion unassigned, 1, > 8, peptide match preferred, exclude isotopes on, and dynamic exclusion of 20 s. Raw data were analyzed by MaxQuant software version 1.6.2.1 and peptide list searched against the *Homo sapiens* Uniprot protein sequence database including isoforms (February 2016, only reviewed entries appended with common laboratory contaminants [cRAP database, 247 entries]) using the Andromeda search engine. The following settings were applied: trypsin (specificity set as C-terminal to arginine and lysine) with up to two missed cleavages, mass tolerances set to 20 ppm for the first search and 4.5 ppm for the second search. Oxidation of M, acetylation of N-termini, phosphorylation of STY, ubiquitination (GlyGly) and acetylation at K, were set as variable modifications and propionylation of cysteine as static modification. False discovery rate (FDR) was set to 1% on peptide and protein level and was determined by searching a reverse database. Peptide identification was performed with an allowed initial precursor mass deviation up to 7 ppm and an allowed fragment mass deviation of 20 ppm. For all other search parameters, the default settings were used. Label-free quantification was done using the XIC-based in-built label-free quantification (LFQ) algorithm integrated into MaxQuant. Spectra for identified modified peptides were manually validated. For FLEXITau SRM experiments, flex-peptide was spiked in to PHF digests (final concentration of 0.05 pmol/uL and targeted LC-MS/MS was performed using the microflow FLEXITau method as outlined above for the Tau sarkosyl fractions.

QUANTIFICATION AND STATISTICAL ANALYSIS

Data was tidied up using tidyverse (1.3.1), dyplr (0.8.5), reshape2 (1.4.2), FactoMinR (2.1) (Lê et al., 2008), plyr (1.8.6) and Microsoft Excel. Statistical data analysis was carried out using a combination of Prism 8.132, Perseus, and R programming language (3.2.1, 3.4,

Please cite this article in press as: Wesseling et al., Tau PTM Profiles Identify Patient Heterogeneity and Stages of Alzheimer's Disease, Cell (2020), https://doi.org/10.1016/j.cell.2020.10.029

3.5.1, and 3.6.0). In R several packages were used. GGplot2 (3.1.1) and pcaMethods (1.78.0) (Stacklies et al., 2007) were used for principal component analysis plots, OPLS-DA plots were generated using ropls (1.18.1) (Thévenot et al., 2015); pheatmap (1.0.8), heatmaply (1.0.), d3heatmap (0.6.1.2) for plotting heatmaps and data exploration, FactorMineR (2.1) (Lê et al., 2008) to calculate PCA confidence ellipses and plot colors were generated using RColorBrewer (1.1.-2) for initial color palettes. The package gradDescentR (1.1.1) was used for building the classifier using stochastic gradient descent. The shinyBS (R package version 0.20) was employed for initial visualizations. Plot colors and plot layout and sizes were finalized using inkscape. For Hierarchical clustering – Euclidean distance was used with a complete clustering of rows.

Supplemental Figures

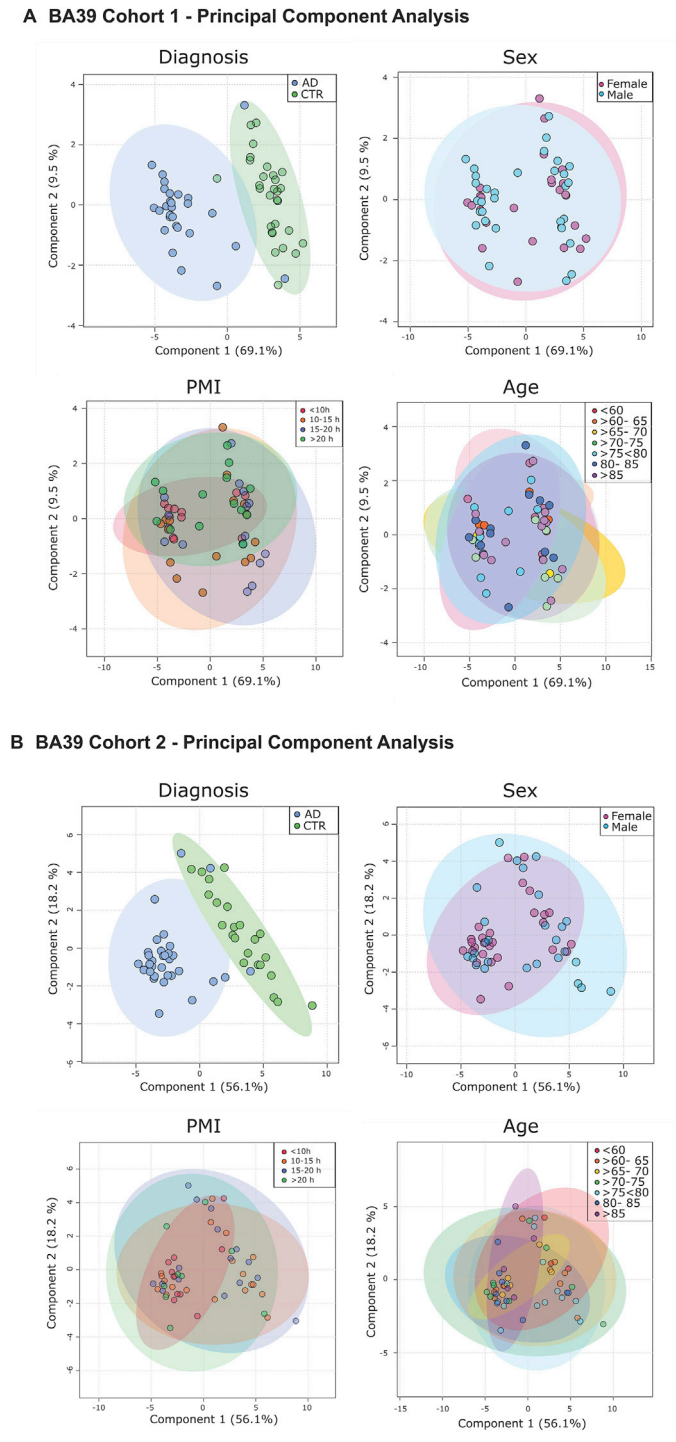

Figure S1. PCA of the Tau PTM Profile (FLEXITau) Separates AD Patients and Control Subjects in Cohort 1 and Cohort 2, Related to Figures 2 and 3

No significant separation is observed on the basis of sex, PMI and age using Tau modification profile data from FLEXITau across both cohorts.

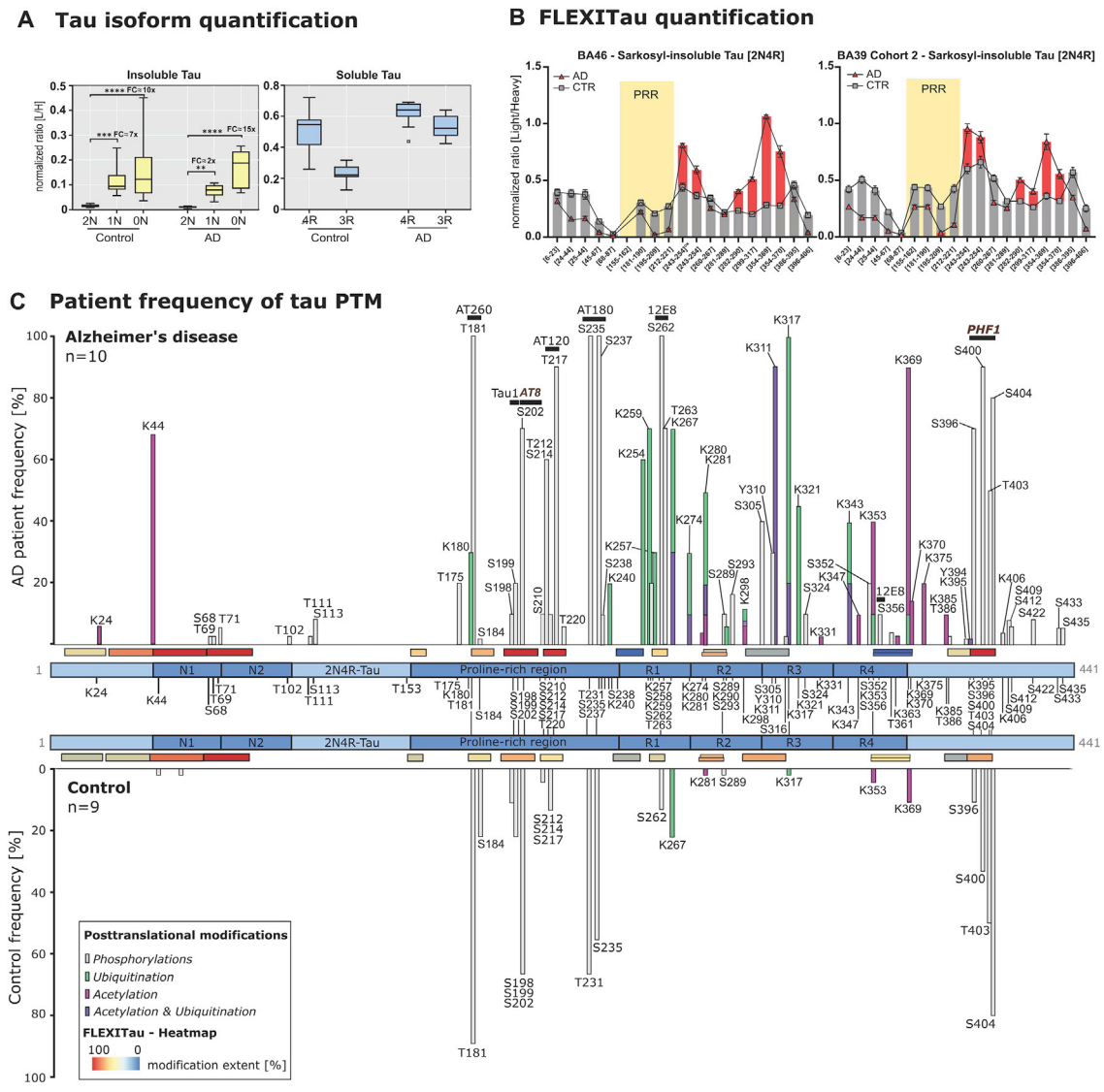

(legend on next page)

Figure S2. Molecular Characterization of Isoform Distribution, Tau Peptide PTMs, and Stoichiometry of Sarkosyl-Insoluble Tau Extracted from Postmortem Frontal Gyrus Tissues (BA46), Related to Figures 1 and 3

A) The isoforms observed in the sarkosyl insoluble Tau from human BA46 tissue is similar to that observed in BA39 angular gyrus tissue (see also Figure 1B). Pathogenic Tau aggregates in AD are predominately composed of 0N and 1N isoforms (yellow boxplot) and the 4R isoform (blue boxplot) in both brain regions. Peptides were quantified using heavy-isotope labeled isoform-specific peptides, and an ANOVA analysis (Kruskal-Wallis) was performed using the Dunn's test for multiple comparisons. Fold changes were calculated based on the mean concentrations measured. B) Side by side analysis of FLEXITau quantified peptides listed from N-C termini in the frontal gyrus and the angular gyrus shows that the Tau modification fingerprint is similar between both regions. C) Patient frequencies of PTMs from the N- to C terminus of Tau in BA46 recapitulate the PTMs and frequencies identified in the BA39 brain region, with four PTMs only detected in BA46 (for comparison refer to Table S5). D) Unsupervised Euclidian hierarchical clustering analysis of Tau peptides measured using FLEXITau in BA46 separates AD and control patients and reflects the BA39 analysis with most discriminative peptide features being the R3-R4 in the MBD and the PRR domain (see also Figure 2A). The left panel clusters the samples and peptides using Euclidian distance, whereas the right panel shows the peptides sorted by their position within the 2N4R sequence of Tau.

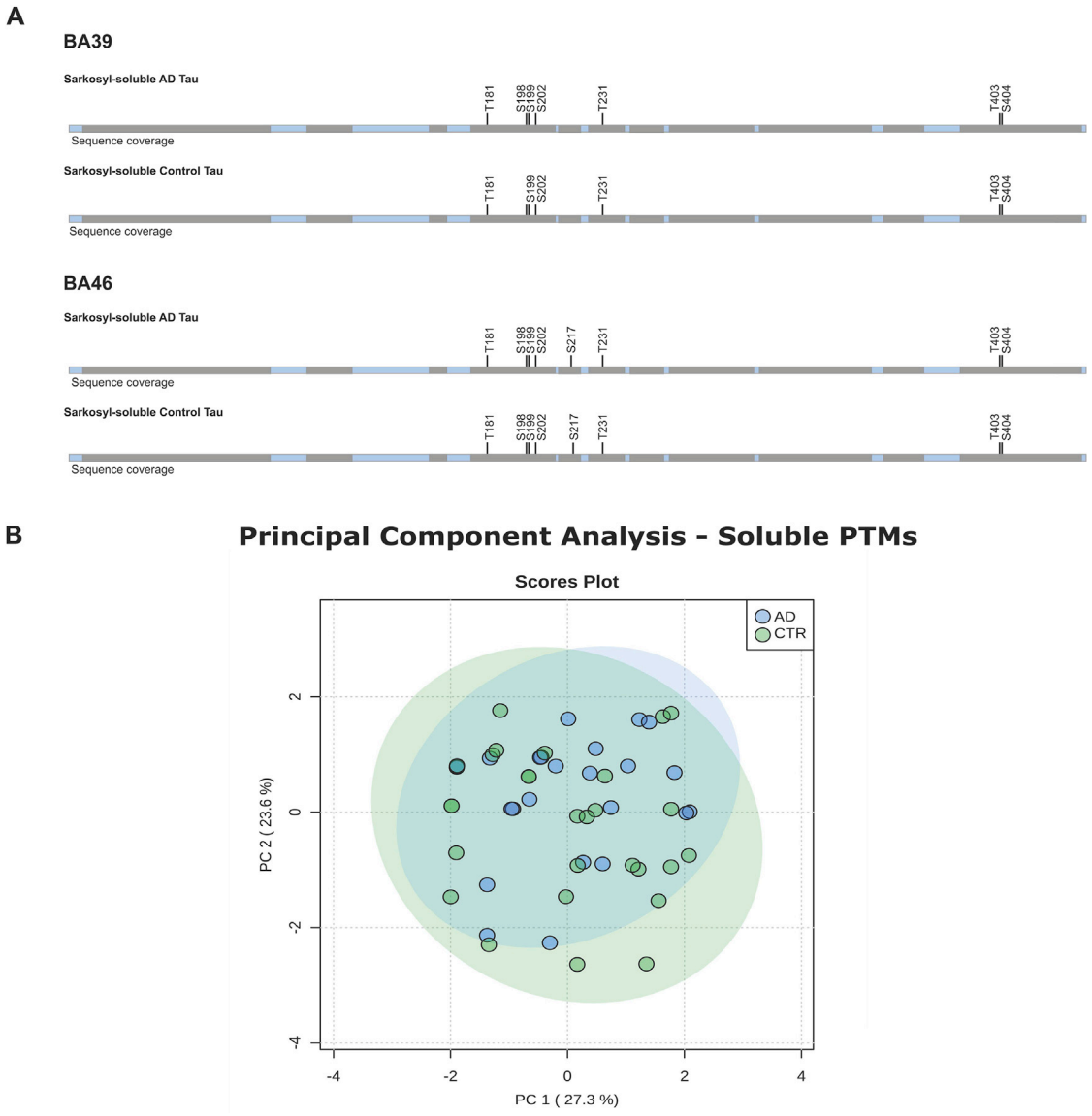

Figure S3. Analysis of the PTM Landscape of Sarkosyl-Soluble Tau from AD Patients and Matched Controls, Related to Figures 2, 3, and 4D

A) PTMs mapped on sarkosyl soluble Tau extracted from angular gyrus (BA39) and frontal gyrus (BA46) tissue shows that PTMs associated with physiological function dominate the profiles for both AD and control subjects. B) PCA does not separate the patients and control subjects based on the soluble modified tau peptides (sarkosyl soluble fraction) extracted from angular gyrus (BA39) tissue.

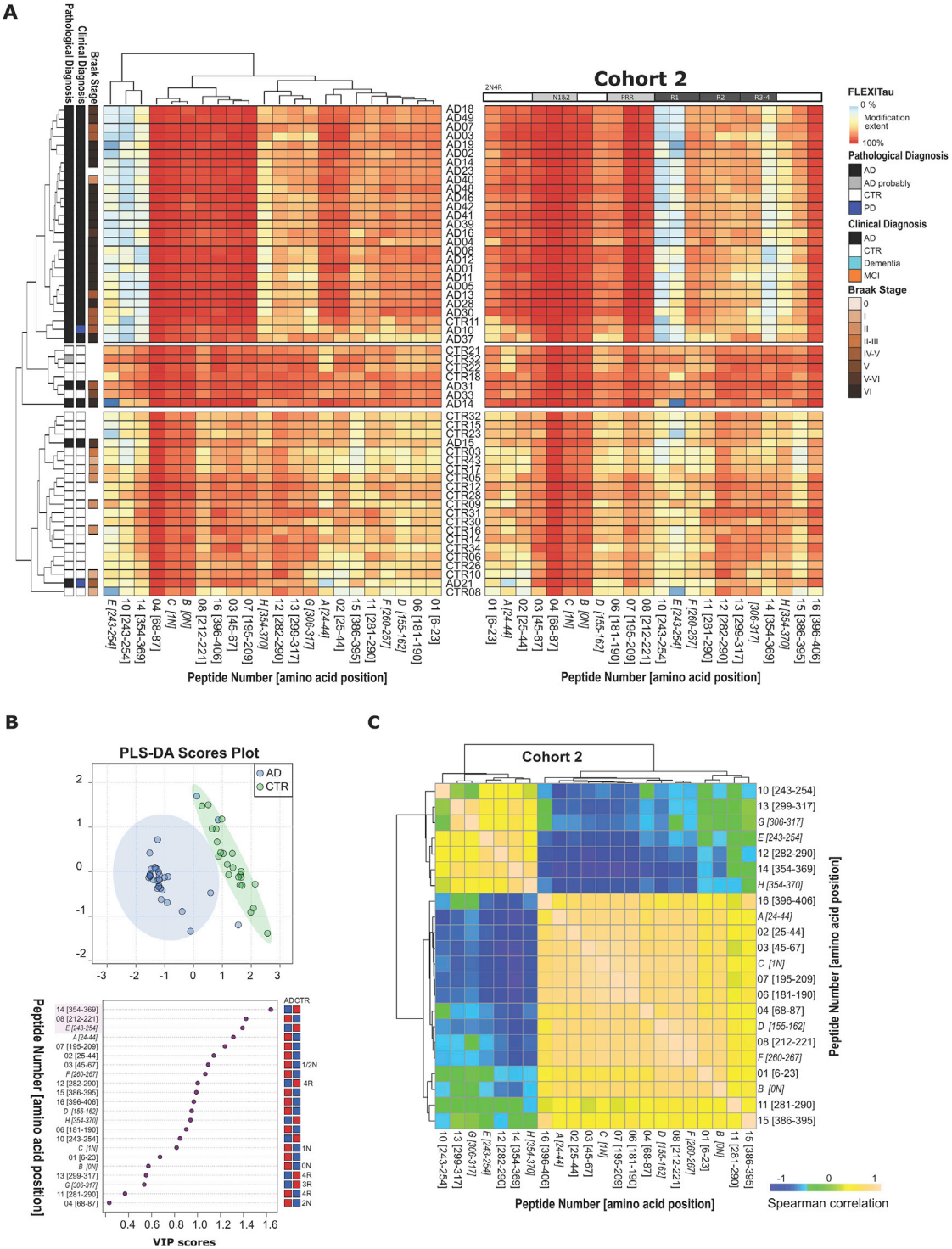

Figure S4. FLEXITau Cohort 2 of ADPatients and Age-Matched Control Subjects, Related to Figure 3

(A) Hierarchical clustering of Tau peptides measured using FLEXITau in cohort 2. Peptides in the left heatmap are sorted by the 2N4R Tau sequence, whereas hierarchical clustering analysis was performed on the peptides of the right heatmap. (B) Supervised PLS-DA analysis of the FLEXITau peptide modification extent separates the subjects according to their pathological diagnosis and identifies three peptides to be most discriminative (VIP scores plot), which are validated across the cohorts. (C) Spearman correlation analysis shows that the PRR and 1N/2N specific peptides are anti correlated with an increase abundance in the MBD in cohort 2.

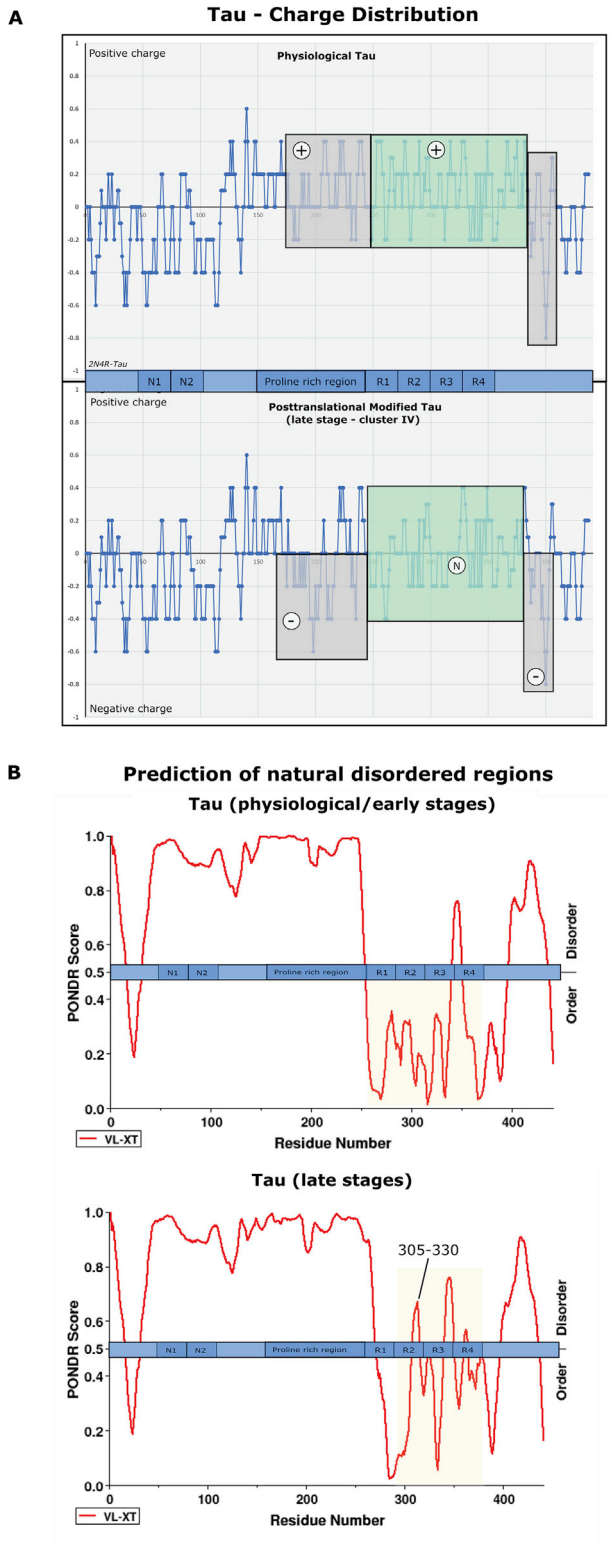

Figure S5. Related to Figure 5

(A) Charge distribution of 2N4R Tau shows that the PTMs in the late stage of the disease neutralize the positive charges in the MBD and add negative charge in the PRR region. (B) Prediction of natural disordered regions demonstrates that MBD domain becomes increasingly disordered from aa 305-330 which is ubiquitinated in the late stage of AD.